Synthesis and Study of Electrical and Mechanical Properties of Polypyrrole/SIS Copolymer Blends and Bimetallic Polymeric Nanocomposites

Fareaa Batool

Reg. # 00000117137

A dissertation submitted in partial fulfillment of requirements for the

Degree of Master of Science in Chemistry

Supervised by

Dr. Faroha Liaqat

Department of Chemistry

School of Natural Sciences

National University of Sciences and Technology

Islamabad, Pakistan

2017

National University of Sciences & Technology

MS THESIS WORK

We hereby recommend that the dissertation prepared under our supervision by: Fareaa Batool, Regn No. 00000117137 Titled: Synthesis and Study of Electrical and Mechanical Properties of Polypyrrole/SIS Copolymer Blends and Bimetallic Polymeric Nanocomposites be accepted in partial fulfillment of the requirements for the award of **MS** degree.

Examination Committee Members

1. Name: PROF. HABIB NASIR   Signature: _____

2. Name: DR. FAHAD EHSAN   Signature: _____

3. Name: _____   Signature: _____

4. Name: DR. SAIMA SHABBIR   Signature: _____

Supervisor's Name: DR. FAROHA LIAQAT   Signature: _____

_____
Head of Department

25-08-17
Date

COUNTERSINGED

Date: 25/8/17

Dean/Principal

THESIS ACCEPTANCE CERTIFICATE

Certified that final copy of MS thesis written by **Ms. Fareaa Batool**, (Registration No. **00000117137**), of **School of Natural Sciences** has been vetted by undersigned, found complete in all respects as per NUST statutes/regulations, is free of plagiarism, errors, and mistakes and is accepted as partial fulfillment for award of MS/M.Phil degree. It is further certified that necessary amendments as pointed out by GEC members and external examiner of the scholar have also been incorporated in the said thesis.
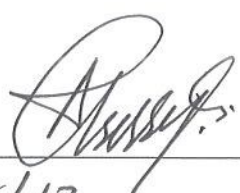
Signature: _____

Name of Supervisor: Dr. Faroha Liaqat

Date: _____ 25. 08. 17 _____

Signature (HoD): _____

Date: _____ 25 - 08 - 17 _____

Signature (Dean/Principal): _____

Date: _____ 25/8/17 _____

In the Name of Allah, The most Gracious, and The most Merciful

"O my Lord! Increase me in knowledge." (Quran 20:114)

***Dedicated to**

My loving grandmother, parents and sisters

Table of Contents

5

CHAPTER 3

3.   RESULTS AND DISCUSSION

Abbreviations and Symbols

ASTM	American Society for Testing and Materials
CB	Conducting band
CPs	Conducting polymers
DTAB	Dodecyltrimethyl ammonium bromide
DMF	Dimethyformamide
DNA	Deoxyribonucleic acid
EC	Epicatechin
ECG	Epicatechin-3-gallate
EGC	Epigallocatechin
EGCG	Epigallocatechin-3-galla
eV	Electron Volt
FTIR	Fourier transform infrared spectroscopy
HPC	Hydroxylpropyl cellulose
HOMO	Highest occupied molecular orbital
LUMO	Lowest unoccupied molecular orbital
HMPSAS	Hot melt pressure sensitive adhesives
MPa	Mega Pascal
MgO	Magnesium oxide
1D	One dimensional

PPO	Poly (phenylene oxide)
PP	Polypropylene
PA	Polyamide
PPy	Polypyrrole
PVC	Polyvinyl chloride
PANI	Polyaniline
$PdCl_2$	Palladium chloride
SBS	Poly (styrene-butadiene-styrene)
SIS	Poly (styrene-isoprene-styrene)
ClO_4^-	Perchlorate anion
$K_2S_2O_8$	Potassium peroxodisulfate
RNA	Ribonucleic acid
SDS	Sodium dodecyl sulfate
SEM	Scanning electron microscopy
$AgNO_3$	Silver nitrate
T_m	True melt temperature
TEM	Transmission electron microscopy
TGA	Thermal gravimetric analysis
VB	Valence band

LIST of FIGURES

LIST of TABLES

Acknowledgements

Abstract

Conductive polymers such as polypyrrole, polythiophene and polyaniline have received significant attention because of their outstanding and attractive electronic, optical, conductive and redox properties. Among all conducting polymers, polypyrrole has gained greater interest due to its high conductivity along with good thermal and environmental stability. Polypyrrole can be easily oxidized both chemically and electrochemically. It (PPy) is widely used in batteries, sensors, super-capacitors, microwave shielding, corrosion protection, electrical wiring coating, and radar absorption. Due to the strong inter and intramolecular interactions and cross linking of PPy chains, it is not soluble in organic solvents and water. Because of its rigid ring structure, polypyrrole is very brittle, inflexible, exhibits poor processability and lacks mechanical or film forming properties.

Stability of polypyrrole films can be achieved by forming blends of polypyrrole with different insulator, thermoplastic copolymers. In this research work blends of polypyrrole have been formed with poly(styrene-isoprene-styrene) (SIS) thermoplastic insulating copolymer by loading polypyrrole within the range of 6-15 wt.%. In SIS copolymer polystyrene has glassy domains dispersed in the flexible polyisoprene matrix, giving an overall flexibility to polypyrrole in blend, enhancing mechanical strength of PPy with the enhancement of electrical conductivity of insulator SIS copolymer. FTIR analysis has confirmed the incorporation of polypyrrole in to SIS copolymer. Electrical conductivity of blends was measured by two-point method and mechanical properties were determined through mechanical testing of each blend. Enhancement in electrical conductivity and mechanical properties was reported with the increase in PPy loading into SIS copolymer and the best results were obtained with 15 wt% PPy/SIS blend.

Conductivity and mechanical strength of 15 wt. % PPy/SIS blend was tremendously increased further by the addition of Ag-Pd bimetallic nanoparticles as nanofiller. A novel ecofriendly, green technique was used for the synthesis of Ag-Pd bimetallic nanoparticles. In this work, *Camellia sinensis* (green tea) extract was used for the first time to synthesized bimetallic Ag-Pd. XRD analysis has confirmed the pure Ag-Pd bimetallic nanoparticles were synthesized with an average crystallite size of 7.9 nm.

FTIR analysis indicates the presence of different capping agents over the surface of synthesized nanoparticles. Elemental composition of synthesized nanoparticles was determined by EDX analysis. In order to enhance mechanical and electrical properties of 15 wt. % PPy/SIS blend, Ag-Pd bimetallic nanoparticles were loaded within the range of 1-5 wt. % to form nanocomposites. Enhancement in the electrical and mechanical properties was observed with the increasing amount of Ag-Pd nanoparticles.

Chapter 1

Introduction

Polymer is combination of two words "Poly" means "many" and "mer" means "parts". Polymer is basically combination of small repeating units, monomers that link together to form large molecules.The process by which the monomers combine to form polymer is known as polymerization [1]. Polymers can be natural as well as synthetic. Natural polymers exist in nature in the form of DNA, proteins, RNA, carbohydrates since the life began. Thomas Hancock and Charles Goodyear have modified natural rubber through blending and vulcanization using sulfur and the first synthetic polymer, Bakelite was produced in 1909[2]. On the basis of different chemical, physical, thermal properties, polymers can be classified in different ways, which are summarized in Table 1.1.

Table 1.1: Classification of Polymers on Different Basis

Basis of Classification	Type of Polymer
Origin	Synthetic polymer, semi synthetic and Natural polymers
Thermal Behaviour	Thermoplastic polymer, Thermosetting polymer
Mode of Formation	Addition , Condensation
Line Structure	Linear, Branched, Cross-linked
Physical Properties	Rubber, Fiber, Plastic
Tacticity	Isotactic,Syndiotactic, Atactic
Crystallinity	Amorphous, Semi-crystalline, Crystalline
Polarity	Polar, Non polar
Chain	Heterochain, Homochain

On the basis of thermal response there are two types of polymers such as thermoplastics and thermosets. Those polymers that can soften on heating and can be molded into a desired form are called *thermoplastics*.

In comparison*,* such polymers which have covalently bonded cross linked structure. Once formed, these cross linked networks show resistance toward heat softening and can not be remolded are called thermosets once set, set forever [3].

1.1   Conducting Polymers

Conducting polymers have an aromatic ring or conjugation in polymer backbone which facilitates the delocalization of electron to conduct electricity by the addition of small amount of dopant [4]. Dopants are used in conducting polymer to increase conductivity up to of 10^5 S/cm, either by reduction or oxidation reaction. Conducting polymers are very attractive due to their wide range of electrical conductivity, which can be achieved by various doping level, while maintaining their mechanical and thermal stability. Electrical conductivity of CPs is affected by mobility as well as density of charge carriers, presence of doping material and temperature. Conducting polymers are different from polymers filled with carbon black or metal, since the latter are only conductive if the individual conductive particles are mutually in contact and form a coherent phase [5]. Conducting polymers are frequently called ''synthetic metals'' because they present electric as well as magnetic properties inherent to metals or semiconductors, while retain the mechanical properties of conventional polymers [6]. Important conducting polymers are poly(*p*-phenylene), polythiophene, poly(*p*-phenylene vinylene), polypyrrole, polyaniline, *trans*-polyacetylene, given in Figure 1.1.
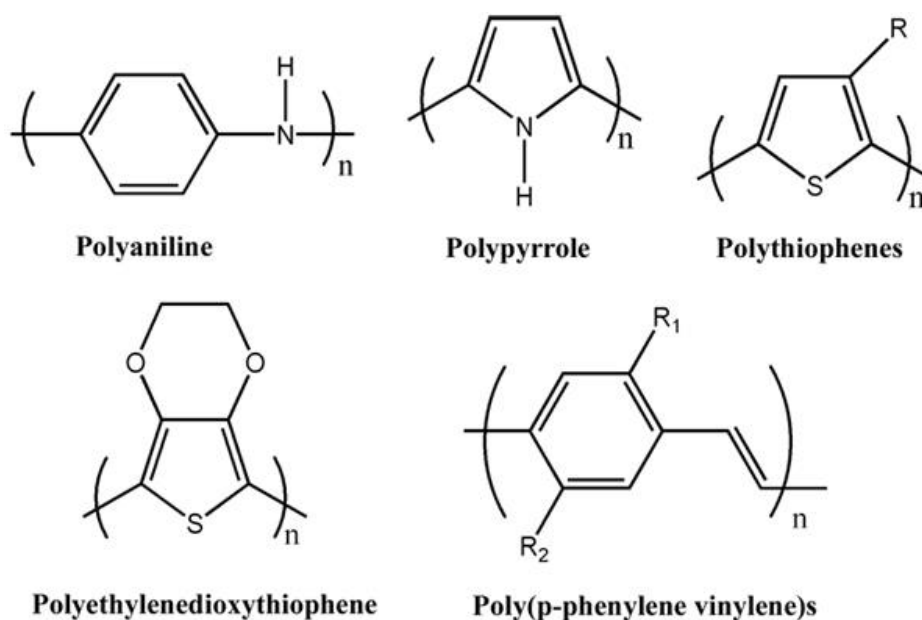
Figure 1.1 Conducting Polymers

An important conducting polymer is **polyphenylene** that comprises of carbon-carbon single bonded phenylene units linked to give linear polymers having an aromatic backbone. Polyphenylene has high melting point, insoluble in most solvents, and stable up to 500-600 °C. Another important CP is **polyaniline** (PANI). Polyaniline is a CP of the semi-flexible rod polymer family. Among all the above classes PANI is of much importance worldwide because of its unique properties. Henry Lethe in the mid-19th century, first time obtained PANI by studying electrochemical and chemical production of aniline in acidic medium [7]. **Polythiophene** (PTh) has been considered one of the most auspicious π-conjugated conducting polymers due to its high stability, relative ease of structural modification and controllable optical along with electrochemical properties. Polythiophene has thiophene or sulfur heterocycle in its polymeric backbone. PTh derivative was reported by two scientists at the Bayer AG research laboratories in Germany in 1980 [8].

Polyacetylene is an important polymer with the $(C_2H_2)_n$ repeating unit. It was the first polymer capable of conducting electricity and was accidentally discovered by Shirakawa in the mid 1970s [9]. **Poly (phenylene vinylene)** PPV is diamagnetic, highly crystalline, mechanically and environmentally stable and has a structure intermediate between that of PA and PP. PPV has extremely low electrical conductivity, which can be enhanced by using iodine, ferric chloride, alkali metals, as a dopant [10]. **Polypyrrole** is a type of organic polymer formed by polymerization of pyrrole. It was reported as CP in 1968. Polypyrrole has gained considerable interest due to its high conductivity along with good thermal and environmental stability and can be easily oxidized both chemically and electrochemically [11]. Almost all conducting polymers have limited solubility due to the presence of bulky ring in its structure.

There is a prevalent misconception that all polymers are plastic, insulator in nature and do not conduct electricity. However this view has been changed by three scientists, USA Professor **Alan G. MacDiarmid** , Professor **Hideki Shirakawa** and Professor **Alan J. Heeger,** discovered that polyacetylene can be made conductor like metal [12].

In 1862 H. Letheby obtained a partially conductive polyaniline by anodic oxidation of its monomer, aniline in sulphuric acid [13]. In 1970s superconductive nature of poly (sulphur nitride) was reported remarkably at low temperature (T_c=0.26 K). However, discovery of polyacetylene was a milestone in the field of conducting polymers [14].

In 1974 Shirakawa and co-workers prepared polyacetylene by using Ziegler-Natta catalyst for polymerization of acetylene, but this alone was not conductor. In 1977, Hideki Shirakawa, Alan G. MacDiarmid , Alan J. Heeger discovered that polyacetylene doping with halogens, such as chlorine, bromine or iodine vapor, its insulating nature can be changed to conductor. Polyacetylene films thus obtained were 10^9 times more conducting than original. These three scientists revolutionized the development of electrically conductive polymers and were granted with "Nobel Prize in Chemistry" in 2000 by Royal Swedish Academy of Sciences [12]. Figure 1.2 shows scientists who discovered conducting polymers.

Figure 1.2: Nobel Prize Winners for Discovery of Conducting Polymers

1.2   Electrical Conduction in Polymers

1.2.1   Band Theory

The electronic properties of material can be explained by its electronic model. According to quantum mechanics, there are quantized or specific energy levels of electron in an atom. The degenerate atomic orbital of an atom overlap to form molecular orbitals which are close in energy to each other. In crystal lattice, atoms are closely packed so these molecular orbitals combine to form bands. The highest occupied molecular orbit (HOMO) containing valence electrons are called valance band while the lowest unoccupied molecular orbit (LUMO) either partially filled or empty are called conduction band.

Material can be classified as insulator, semiconductor or conductor on the basis of band gap between conduction and valence band [15]. In case of insulators, the band gap between CB and VB is very high so valance band is completely filled and no electron is in conduction band as electrons do not have sufficient thermal energy at room temperature to overcome the band gap and jump into CB. In case of semiconductors the band gap between VB and CB is small so small fraction of electron with sufficient thermal energy can jump into CB. The conductivity of semiconductors can be enhanced by increasing temperature. Figure 1.3 shows band theory model [15].
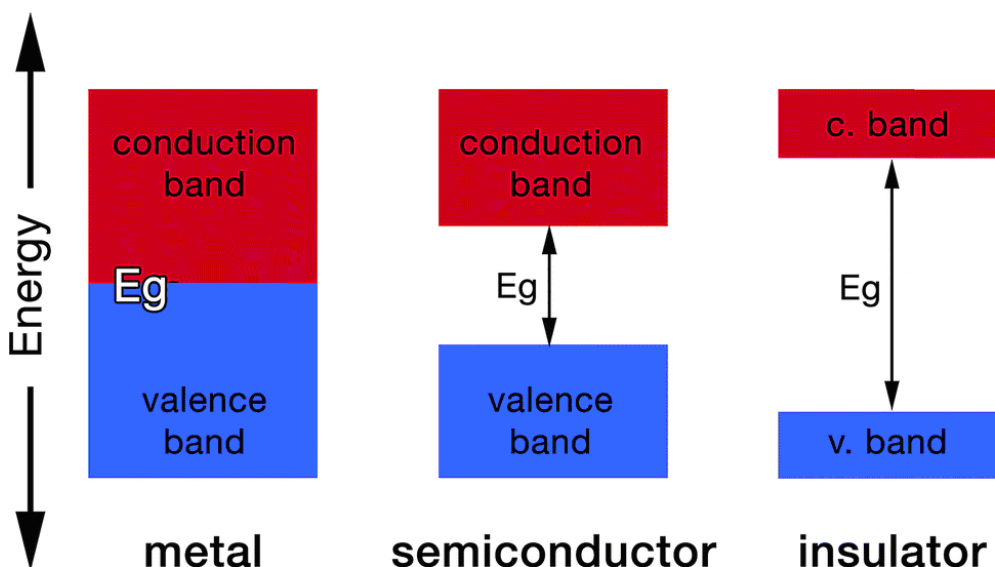
Figure 1.3: Band Theory Model

In case of conductors there is no band gap between VB and CB so the electrons can easily move from VB to CB leading to high conductivity. In case of conjugated polymers when they are in the intrinsic state, have filled valence band and empty conducting band. Mostly the E_g value (Energy difference between HOMO and LUMO) of conjugated polymers is in the range of 1.5-3.0 eV. So the conjugated polymers are semiconductor. This narrow band gap can be changed by doping either by addition of electron to conduction band (n-doping) or by removal of electron from valence band (p-doping). As a result of removal of electron from HOMO of valence band of conjugated polymer, the valence band becomes partially filled with the creation of radical cation [16]. This radical cation (polaron) is responsible for injection of states in to the band gap from bottom of conduction band and top of valence band. Removal of second electron from positive charged chain further lower the total energy due to creation of bipolaron. At high level of doping the localized bipolarons overlap, result in the formation of new energy bands between VB and CB, through which electrons can flow easily as shown in Figure 1.4[17].
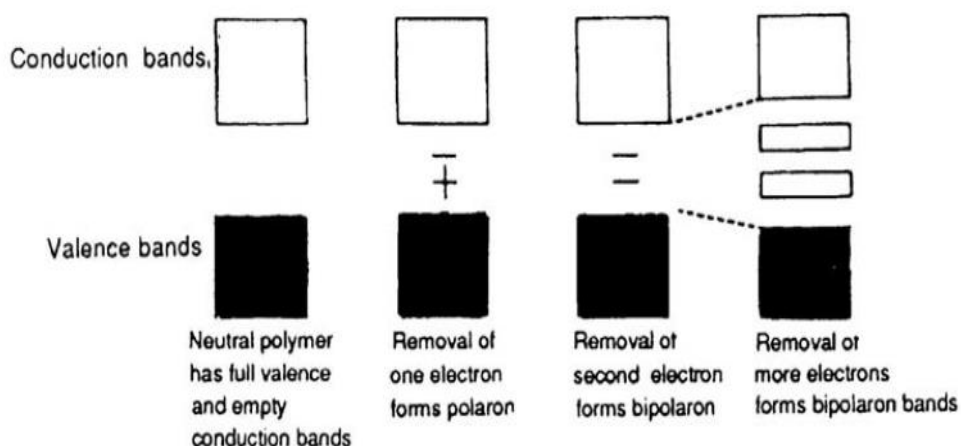
Figure 1.4: Conduction in Conducting Polymers

- **Doping**

Doping is a process of conversion of insulating polymers into good conductors by increasing conductivity of organic polymers to a metallic level either by oxidation 'p-doping' and reduction 'n-doping [18]. In the p-doped state, the polymer backbone is oxidized or loses electrons by the addition p-dopant or oxidants such as I_2, $FeCl_3$, AsF_5 and dopant gains electron to form counter anion. As a result of oxidation, there is excess of holes in polymer chain which makes CP p-type conductive. P-doping of polypyrrole is shown in figure 1.4 where A such as NO_3^-, ClO_4^- or Cl^- behaves as counter anion [15].
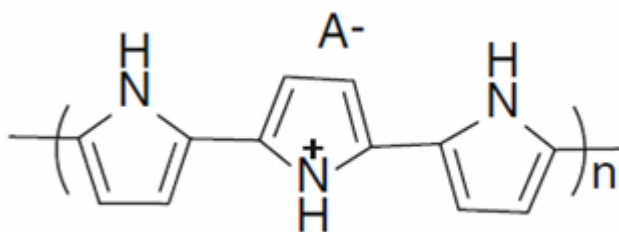
Figure 1.5: P-doped Structure of Polypyrrole

In n-doped state, polymer backbone is reduced to negative charge carrier by the addition of strong reductant such as sodium naphthalide can be used as n-dopant. After doping n-

dopant is oxidized by losing electron to become the counter cation. As a result of reduction, there is an excess of electrons in polymer backbone which makes CP n-type [15].

In this process a charge-transfer complex is formed either by electron donor (Na or K) in case of n-doping or by electron acceptor (I_2, $FeCl_3$, AsF_5) in case of p-doping. The positive or negative charges appear on the doped polymer backbone along with oppositely charge ions will formed by dopant such as Na^+, K^+, I_3^- , I_5^- , AsF_6^-, $FeCl_4^-$. As a result potential difference will create, causing counter ion to move in and out by applying electrical potential and polymer will switched between doped, conductor, undoped and insulator state [5].
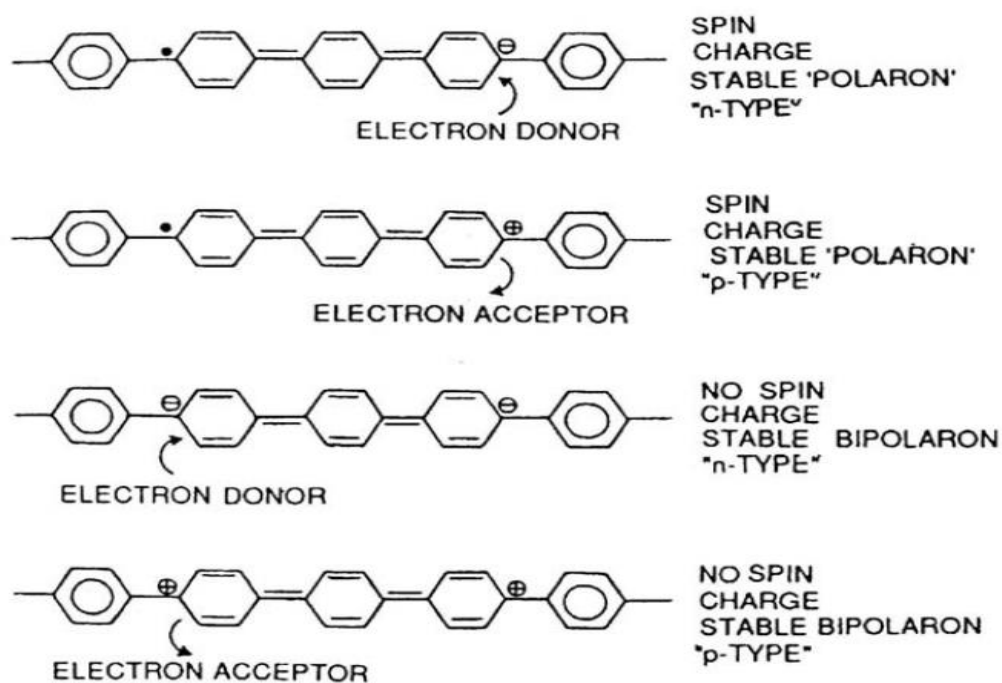
Figure 1.6: n-Type and p-Type Doping in poly-paraphenylene(Polaron and Bipolaron)

Doping in CPs is different from doping in semiconductors. It doesn't involve replacement of bulky atom (such as Si) with n-type or p-type dopant. It involves charge induction by p-type or n-type doping of polymer main chain and neutrality is maintained by counterion

doping. This doping on CPs is also responsible for volume expansion and morphology changes [19].

1.2.2 Polaron and Bipolaron Model

In conducting organic polymers such as polyphenylene or polypyrrole spinless charge carrying species are involved in conduction and band theory is not sufficient to explain conduction. So in this case polaron and bipolaron models are considered to explain conductivity. In conducting polymers charges are stored in different states such as polaron and bipolaron. Polaron is charge carrier defect state that causes to localize the carrier within a potential well produced by the deformation of the molecules in a polymer chain, it occupied. Formation of polaron and bipolaron depends upon level of doping. Polaron formation is due to low doping level while high doping level gives rise to bipolaron. Major charge carrier in CPs is Polaron [5]. Polaron is basically a local distortion in a polymer structure, results from removal of electron. It is a free radical cation or anion that is partially delocalized over several polymer segments.

There are two types of polarons, one are P^+ polarons generated as a result of oxidation of polymer chain and second one are P^- polarons generated due to reduction of polymer chain. They possess ½ spin [19]. Bipolaron is charge carrier that are pair of like charges (such as dication), generated due to coupling of two P^+ or two P^- on a polymer chain. They have no spin and are generated due to high level of polarons on polymer main chain. Polaron and bipolaron are mobile and can move along polymer chain [20]. Band theory of conducting polymers is given in Figure 1.7.[20].
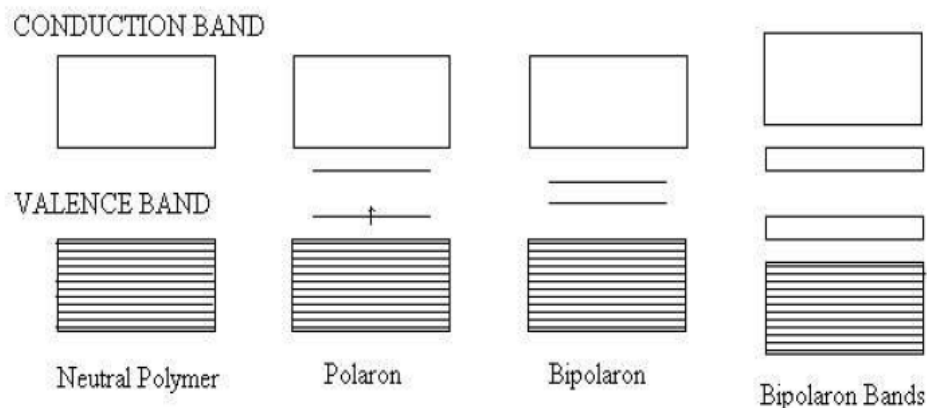
Figure 1.7: Band Theory

Polaron and bipolaron model can be explained by using example of polyaniline given in Figure 1.8.[15]. Generation of polaron is related to removal of electron from CP, creating distortion in polymer structure. When electron is removed from p system, creating free radical and positive charge. Removal of second electron from valence bond generates bipolaron. When electrons removed further or when doping level increased further eventually continuous bipolaron bands with increased band gap and at high level of doping the upper bipolaron band merges with conduction band and lower bipolaron band merges with valence band to produce metallic like conductivity [15].
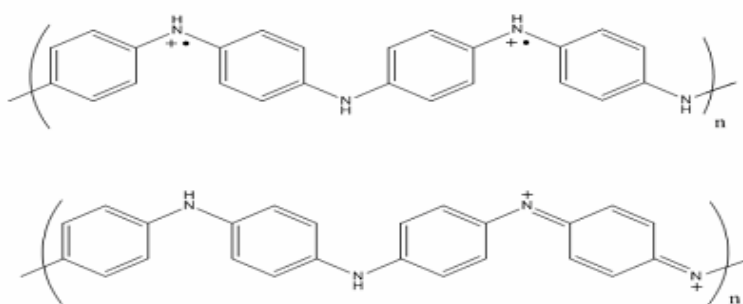
Figure 1.8: Polaron and Bipolaron forms of Polyaniline

1.3 Polypyrrole as Conducting Polymer

Polypyrrole is an important conducting polymer formed by the polymerization of pyrrole. Pyrrole is heterocyclic compound containing five member ring (C_4H_4NH). It has gained considerable interest in recent years due to its ease of polymerization, high electrical

conductivity and good thermal stability [21]. Polypyrrole was earlier known as pyrrole black as it was obtained in the form of black powder by oxidative polymerization of pyrrole monomer [22]. It was first synthesized by oxidative polymerization in 1888 and in 1957 electro polymerization of pyrrole was successfully done to obtain polypyrrole. However its conductive nature was first studied in 1968 [11].
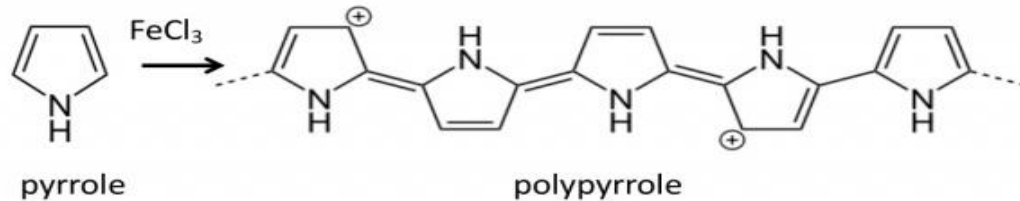
Figure 1.9: Polymerization of Pyrrole

In polypyrrole conduction is due to hopping of charge carriers such as polaron and bipolaron. Neutral PPy has bad gap of 3.16 eV. When dopant is added to polypyrrole, it removes electron from p-system of the polymer backbone resulting a free radical and a spinless positive charge. The radical and spinless positive charge thus produced couple to each other due to local resonance which gives rise to polaron, creating a new localized electronic state. In polypyrrole this polaron state is located about 0.5 eV form the band edge. When oxidation is proceed further, due to high doping level polarons combine and replaced with new spinless state bipolaron located at 0.7 eV from band edge [23].
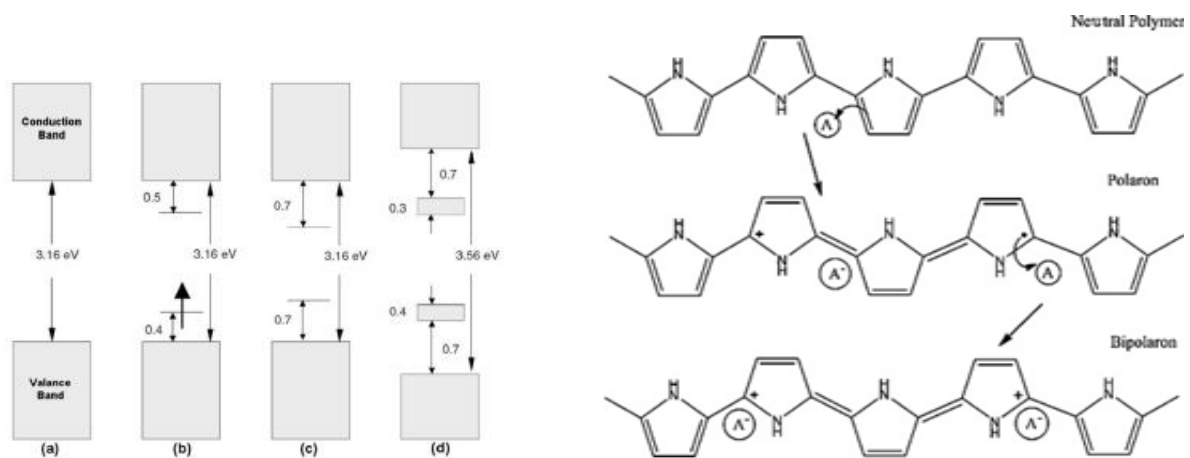
Figure 1.10: Energy level diagram of (a) Neutral PPy, (b) Polaron, (c) Bipolaron, (d) Fully doped PPy.

When doping level is further increased, continuous bipolaron bands with increased band gap are eventually formed. At high level of doping, the upper bipolaron band merges with the conduction band and lower bipolaron band merges with valence band to produce partially filled and metallic like conductivity.

Polypyrrole has a wide range of commercial applications due its electrical conductivity, copolymer and composite forming ability with optimal mechanical properties. It is widely used in batteries, super-capacitors, microwave shielding, corrosion protection, radar absorption material, Sensors, etc. [24]. However due to presence of bulky ring in its structure and strong intermolecular interactions, it is insoluble in different organic solvents and has a poor mechanical properties. This limits its applications in different fields and researchers are trying to overcome this issue by blending, grafting and composite formation [25].

1.3.1   Synthesis of Polypyrrole

Polypyrrole can be synthesized by electrochemical and chemical polymerization. By electrochemical synthesis polypyrrole is obtained as a film deposited on electrodes. It is a complex method and quality and quantity of the film is highly sensitive to pH, concentration of monomer/electrolyte, cell conditions, nature and concentration of solvent, nature of electrodes, voltage applied and temperature [26].

Polypyrrole can also be obtained by enzyme-catalyzed polymerization and photochemical polymerization which involves photo irradiation of PPy using photosensitizer. It is quick and inexpensive method but is not widely developed route [27].

 S.Goel and A. Gupta used time dependent interfacial polymerization to synthesize polypyrrole at the interface of organic and aqueous phase with different dimensions and morphologies. For this purpose they used chloroform as a solvent and oxidizing solution was prepared by dissolving ammonium persulphate in HCl. Polymerization was carried out at the interface of aqueous / organic phase and PPy was obtained as a thin film at interface [28].

Xinyu Zhang and Sanjeev K. Manohar have synthesized polypyrrole nanotubes by chemical oxidative polymerization method. Polymerization of pyrrole monomer was carried out by using ferric chloride as an oxidant and vanadium pantaoxide as the sacrificial template to form long narrow pore-diameter polypyrrole nanotubes with high electrical conductivity [29].

Hongxia Wang and Tong Lin used microemulsion polymerization method to synthesize PPy by using ferric chloride as an oxidant and dodecyltrimethyl ammonium bromide (DTAB) as a surfactant. Effect of various concentration of dodecyltrimethyl ammonium bromide (DTAB) on particle size was also observed i.e. particle size variation from 50 to 100nm and 100 to 200 nm was reported [30].

Yang Liu and Ying Chu used an alcohol assisted microemulsion technique to synthesize polypyrrole by using SDS (Sodium dodecyl sulfate as a surfactant), water as a solvent and aqueous solution of $NH_4S_2O_8$ was used an oxidant. SDS was used to control inner structure of polypyrrole [31].

Masato Amaike and Hiroyuki Yamamot have used emulsion polymerization of pyrrole monomer and hydroxylpropyl cellulose (HPC) to obtain uniform diameter polypyrrole particles. They reported synthesis of water-dispersible polypyrrole. Conductivity of PPy was calculated in the order of 10^{-1} S/cm [32].

M.R. Karim and C.J. Lee have synthesized polypyrrole by radiolysis polymerization which involves in-situ gamma radiation-induced chemical oxidative polymerization for synthesis of PPy. It provided a uniform morphology of PPy polymer [33].

1.3.2 Chemical Polymerization of Pyrrole

Chemical polymerization is the most widely used method for the synthesis of polypyrrole because of its simplicity; it is a   fast process and relatively in-expensive with no need of special instrumentation [34]. Through chemical polymerization polypyrrole is obtained as a black powder. Chemical polymerization takes place by the addition of oxidants, usually $FeCl_3$, $K_2S_2O_8$ and $Fe_2 (SO_4)_3$ to the monomer, pyrrole [35]. Typically monomer and oxidant are dissolved in a solvent at a certain temperature. The mechanism of polymerization has been proposed to be cation-radical polymerization as shown in Figure 1.11[36]. The first initiation step of cation-radical polymerization is oxidation of monomer into a radical cation followed by formation of dimer by coupling of two radical cations.
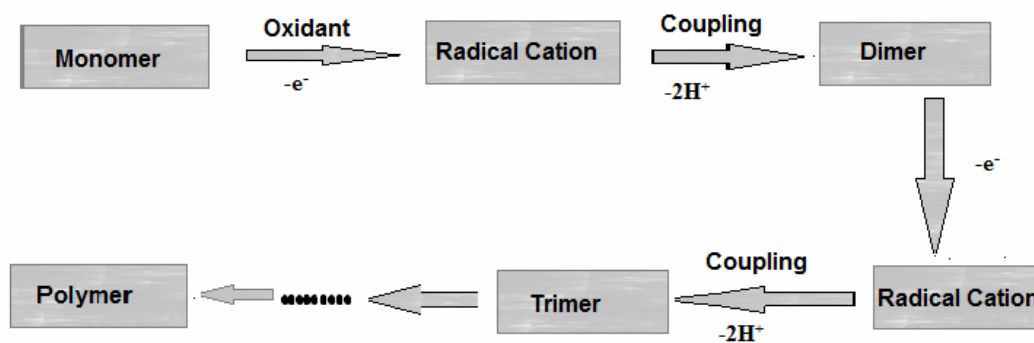
Figure1.11: Scheme of Cation-Radical Polymerization

The dimer is then oxidized to give dimer radical cation and reaction continues until an oligomer is obtained (propagation step). The oligomer finally yields to a polymer followed by termination of chain. The polymer is than filtered, washed and dried [37]. The scheme of polymerization is presented in Figure.1.11.

In the chemical polymerization of pyrrole usually ferric chloride is the best choice of oxidant. During polymerization electro neutrality is maintained by a counter anion created in a reaction mixture by oxidant. For example in case of $FeCl_3$, Cl^- is incorporated

as a counter anion .Chemical polymerization depends upon factors such as solvent, temperature, time, concentration of oxidant etc. These in turn affect conductivity of polypyrrole e.g. Conductivity of polypyrrole increased by decreasing temperature.

A schematic of the chemical polymerization of pyrrole is given in Figure 1.12 [38]. The mechanism of chemical polymerization is similar to electro polymerization. In fist step, pyrrole is oxidized by $FeCl_3$ into radical cation via one electron removal. The radical cation is then coupled with another radical cation followed by loss of two hydrogen ions to give dimer, (2, 2-bipyrrole). This process continues through continuous reoxidation of bipyrrole to form long chains of polypyrrole. When no monomer is left for oxidation , the long polypyrrole chain terminates [38].
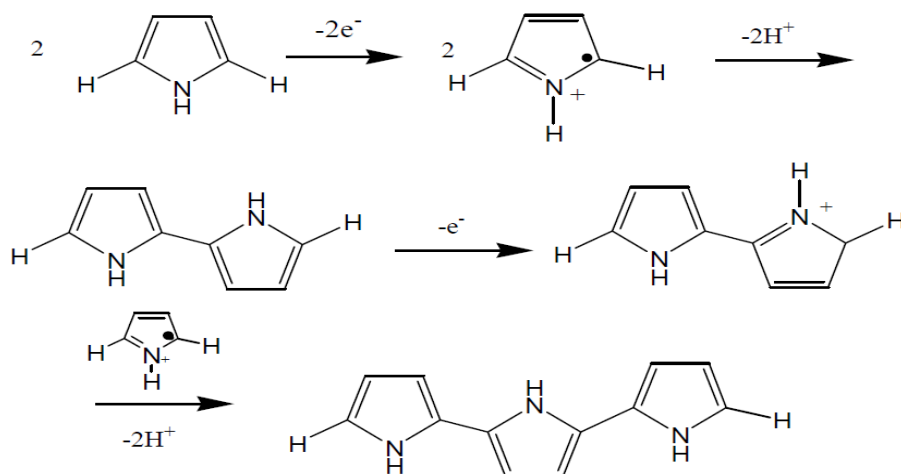
Figure 1.12: Chemical Polymerization of Pyrrole

1.4   Polymer Blends

A polymer blend is a mechanical combination of two polymers to give a new polymer with enhanced properties compared to original components. Polymer blends have gained considerable interest over last twenty years because of low cost and environment friendly. [39].

The fist polymer blend was synthesized by Parkes in 1846. Who synthesized a blend of natural rubber and gutta-percha and obtained a partially cross linked material with enhanced properties [40]. The properties of polymer blends depend upon morphology, contents and properties of both individual components involved in the blend making process. In 1900s, one of the first commercial polymer blend was synthesized by mixing cross linked phenol-formaldehyde polymers with natural rubber. It was used for phonographic records. In early 1940s, parentally plasticized PVC was obtained by mixing PVC and butadiene-acrylonitrile rubber and the blend was used for wire and cable insulation and food packaging films.

Another polymer blend was obtained in 1950s by in-situ polymerization of PS (polystyrene) with rubber to yield poly (acrylonitrile butadiene styrene) with enhanced properties. Until now large numbers of polymer blends have been synthesized with optimum mechanical, electrical and thermal properties [41].

1.4.1   Classification and Methods of Blending

Polymer blends can be classified into the following types:

1. **Immiscible Polymer Blends:** These polymer blends have more than two phases having poor adhesion between them with a large domain of dispersed phase. In this case, two glass transition temperatures will be observed. Examples of fully immiscible blends are polyamide/acrylonitrile butadiene styrene, polyamide/poly(propylene oxide) etc.

2. **Miscible Polymer Blends:** As the name indicates, these blends are a mixture of two polymers that are completely miscible with eachother, having a single phase structure. Therefore, one glass transition temperature will be observed. A well-known example of miscible blend is polystyrene/ poly (propylene oxide) etc.

3. **Compatible Polymer Blends:** These are immiscible polymers blends, have strong interface interaction between polymers blends components. They have in-homogeneity on a small scale and exhibits macroscopically uniform physical

Properties [42].

4. **Compatibilized Polymer Blends:** These are also immiscible blends in which surface active species, compatibilizers, are added to stabilize the physical properties of the blends [42].

- **Methods of Blending**

Blend formation is not a spontaneous process because most of the polymers are immiscible with each other. Methods which are mostly used for blending includes, melt mixing, solution blending, latex mixing, graft copolymerization etc. [43].

Melt mixing is the most widely used method of polymer blending in which two polymers are mixed in molten state in extruders or batch mixers to obtain homogeneous polymer blend. However, this method has certain limitation such as high energy consumption.

As compared to melt mixing solution blending is mostly used on a laboratory level. This is a simple technique which involves blend components and suitable solvents. Both polymers are dissolved in a common solvent e.g. THF, chloroform, DMSO, DMF with continuously stirring. The solvent is then allowed to evaporate in order to obtain pure polymer blend. This technique has advantage over melt mixing because of rapid mixing in less time and less energy consumption. Nowadays a new technique used for polymer blending is solid state shear pulverization also known as cryogenic mechanical alloying. Polymers are grind together below melting temperature by twin screw extruder which provides repeated fragmentation of polymer. By this method, a nanoscale blend is achieved [43].

1.4.2 Polypyrrole Blends- Literature Survey

Polypyrrole is very brittle, insoluble, has poor processability and lacks mechanical properties due to presence of bulky ring in its structure and strong intermolecular interactions, which has limited its applications [32]. However, its mechanical, thermal and electrical properties can be changed by blending with other suitable thermoplastic polymers. Blending is a good alternative to obtain new polymer with enhanced

properties. Through blending the insulating polymer provides high level of processability and brittleness can be overcome [44].

V. Mano, et al [45] synthesized a polypyrrole blend with poly(vinyl chloride) and studied its thermal ,mechanical and electrical behavior. Blends were synthesized by chemical polymerization of pyrrole and exposing PVC impregnated with $FeCl_3$ to pyrrole vapors for 2 hours and 6 hours at ambient temperature. Formation of blend was confirmed by FTIR analysis. It was found that Young's modulus of blend was greatly influenced by exposure time and $FeCl_3$ concentration. Electrochemical properties were studied by cyclic voltammetry that varies from 10^{-4} Scm^{-1} to 10^{-1} Scm^{-1}. Thermal behavior of PPy remained unchanged in case of blending.

Hsing-Lin Wang and Jack E. Fernandez [46] synthesized PPy blend with poly(vinyl methyl ketone) (PVMK) both chemically and electrochemically. They reported that increasing PPy content leads to increased threshold conductivity near 10 %. Hydrogen bonding between both polymers was confirmed by FTIR analysis. By XRD analysis it was reported that crystallinity is independent of polypyrrole concentration in blend. Stability of blends was measured by TGA and it was observed that blends prepared chemically were stable up to 325 ^{O} C temperature while blends prepared electrochemically were stable up to 280 ^{O}C.

S. Baytekin, [47] prepared polypyrrole blend with polypropylene by melt mixing and studied the effect of polypyrrole on mechanical, electrical properties and thermal properties of polypropylene. It was reported that mechanical strength, electrical and thermal behavior of polymer blend increased with the increase in the polypyrrole amount. Electrical conductivity was measured by four point probe and it was increased up to $2,4.10^{-4}$ Scm^{-1} as compared to pure PP. The dispersion of PPy in PP was further improved by using sodium dodecylsulphate as dispersant and enhancement in mechanical, electrical and thermal behavior was reported.

S. Radhakrishnan & D. R. Saini [48] synthesized conducting thermoplastic blends of styrene-butadiene-styrene (SBS) block copolymers with polypyrrole by exposing SBS incorporated with $FeCl_3$ to pyrrole vapors and studied their electrical, mechanical and thermal behaviors. They reported a sharp transition of electrical resistivity at 273 K. All these measurements were on the basis of heterogeneous blend between highly conducting and insulating matrix.

Hsing Lin Wang, et al [49] prepared blends of polythiophene and polypyrrole with insulating polymers, polystyrene and polycarbonate resin. They reported threshold conductivity at 18 wt % concentration of both conducting polymers in case of blend with PS while in case of PC the threshold conductivity was at 12 wt% for Polythiophene/Polycarbonate blend. Low value of threshold conductivity in case of PPy/Polycarbonate was due to homogeneity caused by hydrogen bonding.

S. Hossein Hosseini and Ali A. Entezami [50] prepared Polypyrrole blends with three insulating polymers, polyvinyl acetate (PVAc), polystyrene (PS), and polyvinyl chloride (PVC) and reported their sensing behavior for different toxic gases. Formation of blends was confirmed by FTIR analysis and conductivity was measured by four point probe and it was reported that for 1/3 molar ratios of $FeCl_3$/PPy the conductivity was 4.2E-3, 3.6 E-3 and 0.01 S/cm for PPy/polyvinyl acetate, PPy/Polystyrene, and PPy/Polyvinyl chloride blends respectively.

1.5   Copolymer

Polymers with desirable properties can be obtained by combining two or three monomers to form a copolymer. The sequence of monomers in a copolymer depends upon their relative reactivity and it could be random or alternating. Block copolymers are synthesized by different polymerization techniques and do not occur naturally.
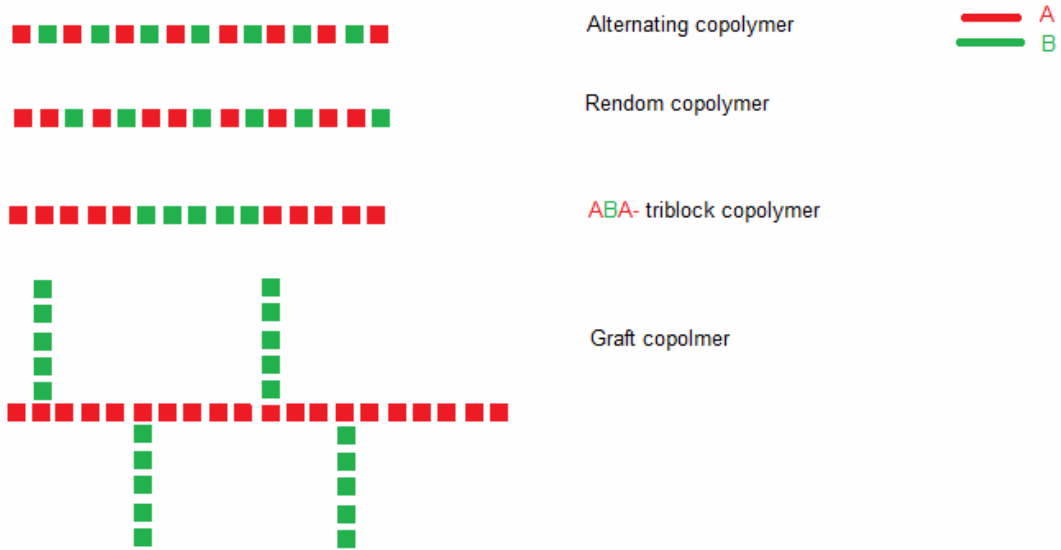
Figure 1.13: Types of Copolymer

Monomers can linked to form ABA-triblock copolymer, in which a long block of monomer A is followed by a block of monomer B and is linked with two A block from both ends

The first ABA block copolymer was prepared by addition of propylene oxide to ethylene oxide having hydrophobic propylene oxide segment and hydrophilic ethylene block segment. It was used as surfactant and formed micelles in aqueous medium with hydrophobic part at core and hydrophilic part oriented outside [51].

Examples of ABA-copolymer include; polystyrene-*block*-polybutadiene-*block*-polystyrene, polystyrene-*block*-polyisoprene-*block*-polystyrene, etc. These are thermoplastic copolymers. Since the mid-1960s, a large number of thermoplastic elastomers were developed. Initially they were derived from plasticized PVC and were known as Plastisols. Thermoplastic elastomers are composed of distinct soft and hard phases. Hard segments are crystalline in nature while soft segments are amorphous in nature. In case of SBS copolymer styrene is crystalline and hard segment, while butadiene is soft and amorphous segment [51].

Copolymers that can not be separated in to individual components are composed of polymers with diverse properties. For example block copolymer of styrene and

methacrylic acid has good solubility in polar as well as in no-polar solvents. .Acrylic acid component extends in polar solvent while it is coiled in non-polar solvent. Each segment of copolymer has its own salient features and characteristic glass transition temperature [3].

1.5.1   Structure and Properties of SIS Copolymer

SIS copolymer also known as polystyrene-block-polyisoprene-block-polystyrene is an ABA triblock copolymer composed of covalently bonded macromolecules such as block of polystyrene connected with block of polyisoprene [52].
 It is highly flexible with high elasticity and has a glassy-rubbery-glassy type composition in which rubbery phase gives overall flexibility to copolymer since both ends of rubbery matrix are attached to a glassy domain which makes SIS a mechanically useful elastomer [53]. Hard and soft segments of SIS copolymer is shown in Figure 1.14 .
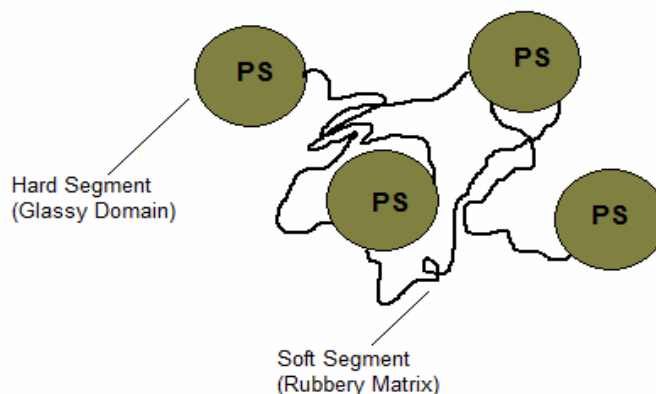
Figure 1.14: Soft and Hard Segments in SIS Copolymer

Polystyrene is a transparent synthetic polymer synthesized by polymerization of styrene monomer and has a low melting point. It is a thermoplastic polymer which is glassy at room temperature and stated to flow when heated above its glass transition temperature. It exhibits poor resistance toward water vapors and oxygen. It is rigid, hard and brittle, forming semi crystalline domain that gives strength to copolymer [54]. On the other

hand, polyisoprene is a synthetic version of natural rubber. It is flexible, rubbery and has a nature of a soft segment. Polystyrene allows the rubbery PI portion to respond in elastomeric manner. Heating of copolymer above T_m (true melt temperature) of polystyrene domains allow mobility of a whole chain and on cooling PS domain reforms [3].
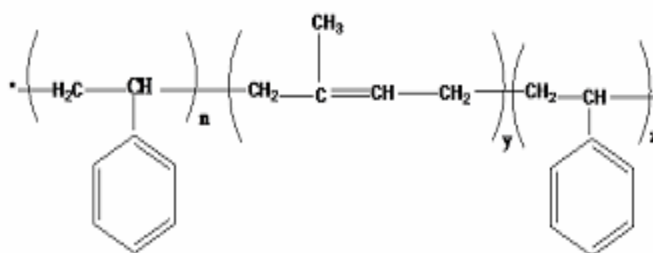
Figure 1.15: Structure of SIS Copolymer

SIS exhibits good film forming properties due to its high elasticity and gives improved properties such as good processability, high compatibility and high aggressive tack (adhesive which are used on textured substrates like wood, corrugated paper or to tire label as they are impossible to remove.) due to which it can be used as pressure sensitive adhesives (HMPSAs). SIS copolymer is soft and its modulus can be increased by increasing styrene in SIS block copolymer. However, high styrene contents give poor elastic and recovery properties. So an optimization has to be achieved between elasticity and modulus [55] . SIS copolymer is soluble in organic solvents with solubility parameters, SI units in delta (δ) between 7.7 and 9.4 such as chloroform, THF etc. It has poor electrical conduction and there exhibits applications as an electrical insulator [56].

1.6   Nanosynthesis of Monometallic and Bimetallic Nanoparticles

The earliest example of nanomaterial usage dates from 4th century when A.D Roman glassmaker, accidentally fabricated a glass named "Lycurgus cup", which was able to change color when exposed to light .This glass was composed of nanoscale metals of silver and gold nanoparticles with a diameter of 70 nm. This fabrication technique was

further used to make "Ruby glass" during medieval ages [57]. In the 18th and 19th century, use of Ag NPs in photography was studied and it was reported that silver halides in a photographic films decomposed to silver nanoparticle when exposed to light which were basically pixel of photographic image [58]. In 1914 particles were first time characterized by Richard Adolf Zsigmondy. He studied gold sols and other nanomaterials up to 10 nm size by using ultra microscope (ulta fine microscope is used to view particles having a diameter close to the wavelength of visible light (around 500 nanometers) [59]. The concept of nano was first introduced to the world by Richard Feynman in 1959 with his lecture "There's plenty of room at the bottom" at American Physics Society meeting. He concluded that it is possible to manipulate things at small scale and this concept gained more strength when the word 'nanotechnology' was used by K. Eric in his book "Engines of creation: The Coming Era of Nanotechnology" [60]. One of the major developments in nanoscience started was invention of Scanning Electron Microscope (SEM) in 1981 by Gerd Binnig and Heinrich Rohrer for surface morphological study of material at nanoscale [61].

Nanotechnology is an emerging field of synthesizing materials in nano dimensions where nano is one-billionth of meter. Nanomaterials are those which have one or more dimensions in nanometer range (1-100 nm) and show unique properties as compared to bulk counterpart [62]. Nonmaterial can be classified into four classes on the basis of dimensions:

1. 0D nanomaterials are those which have no dimension with length larger than 100 nm or all dimensions are with in a nanoscale (1-100 nm) for example nanoparticles, nanoshells , fullerene etc.

2. 1D nanomaterials are those having length larger than 100 nm at least in one direction e.g. thin films, surface coating etc [63].

3. 2D nanomaterials are those having length larger than 100 nm at least in two dimensions with in nanometer range. For example nanotubes, dendrites, nanowires etc.

4. 3D nanomaterials are those having length greater than 100 nm in all three dimensions . e.g. or nanocrystals, bulk [63].

Bimetallic nanoparticles as the name indicates are composed of two different metals while monometallic nanoparticles are composed of single metal. Bimetallic nanoparticles are preferred over monometallic nanostructures from scientific and technological point of view because of enhanced catalytic properties of original metal by bimetallization that can not be found in monometallic nanoparticles [64].

The most important features of nanoparticles are increased surface area to volume ratio which leads to the increased number of active sites in nanomaterial as compared to bulk. As a result these nanomaterials have wide range of applications in medical, industrial, energy storage, cosmetic as well as in clothing industries [65].

- **Synthesis of Nanoparticles: Different Approaches**

Nanoparticles have been synthesized by various techniques. The two main approaches used to synthesize ultra fine nanoparticles include top-down and bottom up approach as shown in Figure 1.16. In top down approach bulk material is broken down into nanoparticles by applying external force. Top down approaches include milling or attrition, repeated quenching .However, top down approach has certain limitation such as broad size particle distribution with varied geometry. There is a chance of contamination of nanoparticles by impurities during ball milling [66]. Second approach is bottom up approach which involves self assembly of building blocks of (atoms or molecules) to produce nanoparticles. It is a widely used technique for nanoparticles synthesis, which gives uniform particle size distribution with same geometry and greater flexibility. Through bottom up approach monometallic as well as bimetallic nanoparticles can be synthesized chemically as well as biologically.
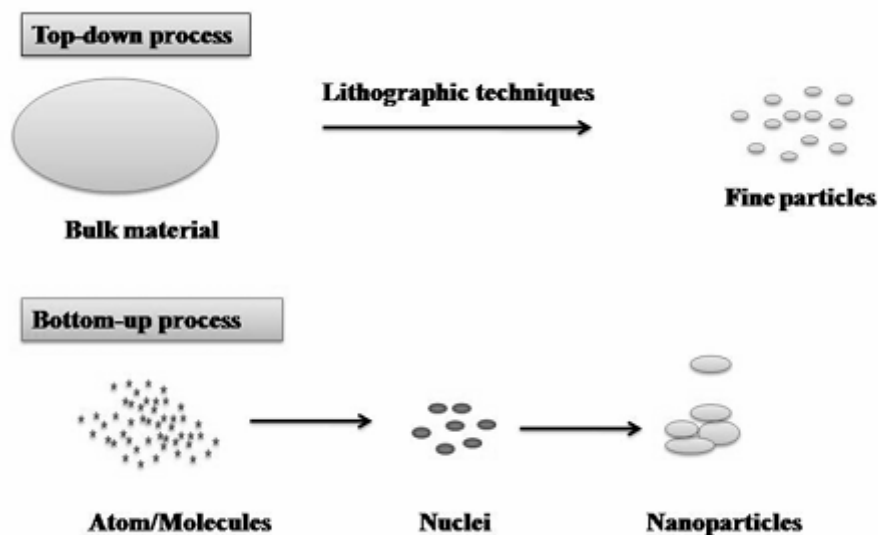
Figure 1.16: Top-down and Bottom-up Approach for Synthesis of Nanoparticles

The Chemical methods can be diverse such as sonochemical, alcohol reduction etc. Chemical methods have certain limitations such as absorbance of toxic chemicals on nanoparticle surface during synthesis of nanoparticles .Another approach towards synthesis of NPs is by green chemistry for example by using biological methods in which microorganisms, enzymes, bacteria, Fungi and different plants extract is used for nanoparticles synthesis [62]. This is an ecofriendly method which eliminates the use products which are harmful to environment as well as ecosystem. The advantages involves in using green chemistry includes , choice of ecofriendly solvent, selection of reducing agent to form complex with metal ,choice of capping agent to control particle size.

Scientists are showing considerable interest in identifying new ecofriendly methods with to synthesize monometallic as well as bimetallic nanoparticles. For example Vitamin B_2 is a good reducing agent with multifunctional properties since it also behaves as a capping agent for nanoparticles. It is less toxic as compare to other reducing agents used in chemical methods e.g. Sodium borohydrate ($NaBH_4$), hydroxylamine hydrochloride, etc [67].

Ecofriendly reducing agents such as vitamin B_2 first form complexes with metals by simultaneous reduction of metal oxides into nanoparticles followed by capping with oxidized vitamin B_2 [67].

1.6.1   Green Synthesis of Monometallic/Bimetallic nanoparticles - Literature Survey

Different plants extract have been used by researchers for the synthesis of nanoparticles because of their ecofriendly nature. In many plants extract, reducing agents first forms a complex with metal atom after simultaneous reduction of metal salts/oxides into nanoparticles followed by capping.

Mallikarjuna N. Nadagouda and Rajender S. Varma have used ascorbic acid (Vitamin C) to obtain bimetallic nanoparticles. They used Fe and Cu transition metal as a core to form bimetallic nanoparticles with noble metals (shell) such as of Cu-Pt, Fe-Au, and Fe-Au, Fe-Pt, Fe-Pd. Depending on the choice of core-shell materials, varying shapes of core-shell nanoparticles were obtained for example, tennis ball like structures of Pt were obtained with Cu core where as regular spherical structures of palladium and gold were formed with Cu. Similarly, when Fe was used as core Au, Pt, Pd formed cube- shapes structure. Core-shell nanoparticles were also obtained by using noble metals as core and transition metal as a shell. When Pd was used as a core, an indium (shell) formed brush like structure while using Cu as a shell formed needle-like structure with Pd (core).These nanoparticles were further characterized by TEM [67].

Yuet Ying Loo, et al used green chemistry to synthesize Ag nanoparticles at room temperature by using Chinese tea, *Camellia sinensis* leaves extract. Nanoparticles were characterized by FTIR, XRD and TEM analysis. TEM images showed that size of the nanoparticles were of 4nm. Highly crystalline spherical shaped Ag nanoparticles were obtained by using *Camellia sinensis.* FTIR analysis has confirmed that polyphenols, carbohydrates and protein on nanoparticle surface were behaving as capping and stabilizing agent [68].

Mallikarjuna N., et al synthesized monometallic palladium and silver nanoparticles by using coffee extract and tea extract at room temperature with out using any surfactant. Nanoparticles were characterized by various techniques such as UV-Vis analysis, XRD and TEM. By this method nanoparticles of 20-60 nm in size range were obtained depending on the source of coffee and tea extract. TEM images showed that Ag nanoparticles were well separated and palladium nanoparticles were well arranged with uniform separation [69].

Gaurav Pant, et al used *Solanum trilobatum Linn* extract for the synthesis of Ag NPs by conventional as well as homogenization method and optimized the situation under sunlight and room temperature. The best results were reported when nanoparticles were synthesized under sunlight, exhibiting 15-20 nm size with cubic and hexagonal shape. High antibacterial activity of silver nanoparticles was reported for different strains. High antifungal activity for dandruff causing fungal pathogens was also reported [70].

Ting Wang, el at used green tea and eucalyptus leaves extracts to synthesize iron nanoparticles and used these for nitrate removal. The synthesized iron nanoparticles were confirmed by FTIR, SEM, EDS and XRD analysis. FTIR analysis confirmed that polyphenols in green tea and eucalyptus leaves are responsible for reduction and stabilization of Fe nanoparticles. Batch experiment has reported that 59.7% and 41.4 % nitrate was removed by Fe nanoparticles obtained by green tea and eucalyptus extract as compared to zero-valent iron nanoparticles. Kinetic of the reaction was also studied and it was reported that the observed nitrate removal process compared well with pseudo-second-order adsorption model. Synthesized Fe nanoparticles showed great potential for nitrate removal from swine wastewater [71].

Khalil Farhadi, et al synthesized core-shell Ag-Pd bimetallic nanoparticles with different ratios using *Acanthe phylum bracteatum* extract by employing galvanic displacement reaction. In this method, palladium chloride reacts with silver nanoparticle containing soap root. The bimetallic nanoparticles were characterized by UV-Visible spectroscopy,

X-ray diffraction, TEM analysis scanning electron microscopy (SEM) with energy-dispersive X-ray spectroscopy (EDX). FTIR and XRD confirmed Ag-Pd bimetallic nanoparticles formation. All the peaks in XRD were in between monometallic Ag and monometallic Pd nanoparticles. TEM analysis showed spherical and uniform shaped bimetallic nanoparticles with 15 nm particle size [72].

Ramesh Kumar Petla, et al prepared palladium nanoparticles by using soybean leaf extract riched with proteins. Synthesized Pd nanoparticles were confirmed by XRD, UV-visible, FTIR and TEM analysis. FTIR confirmed that proteins and aminoacids present in soybean leaves are responsible for reduction and stabilization of nanoparticle. XRD analysis reported face cubic centered nanoparticles and size of nanoparticles were calculated 15 nm by using TEM analysis. Good azo dyes degradation activity of synthesized palladium nanoparticle was also reported [73].

1.7 Nanocomposites

A nano-composite material is formed by the combination of two phases in which at least one of the phase is in nanometer range. Nanocomposites are of different categories but in general, the larger phase is known as the matrix phase while the phase present in small quantity and embedded in the matrix phase is known as reinforced phase. Properties of matrix phase can be intensify by loading nanofillers as reinforcement. Properties of bulk materials can be enhanced by combining with nanoparticles to form nanocomposite [74].
In general nanocomposites are smart alternatives to microcomposites due to their improved mechanical, electrical catalytic, magnetic and optical properties [75]. Nanocomposites have high surface area to volume ratio and due to reduced size of nanofillers present; these nanocomposites are lighter in size as compared to bulk-composite materials [76]. The reinforced phase may be composed of particles such as minerals, nanoparticles, carbon nanotubes or sheets such as exfoliated clay, graphene or fibers such as nanofibers. Control of elemental composition is a big issue when synthesizing nanocomposites. In 1991 carbon nanotubes were discovered and their potential applications in nanocomposites have been vastly exploited [74].

Example of nanocomposite in nature include bone, which is composed of almost 30 % matrix material e.g. collagen fiber and 30 % nano minerals e.g. is hydroxyapatite crystals [77].

1.7.1 General Classification of Nanocomposites

On the basis of reinforce phase and matrix phases, nanocomposites can be classified into different categories such as, Nanoclay-reinforced nanocomposites, Carbon nanotube-reinforced nanocomposites, Nanofibre-reinforced nanocomposites, and Inorganic particle-reinforced nanocomposites, structural reinforced nanocomposites [78]. On the basis of matrix material nanocomposites are classify into three classes:

- **Ceramic Matrix Nanocomposite**

Ceramic matrix nanocomposites are those in which matrix phase is composed of ceramic material such as oxides, nitrides and silicates. They have wide range pf applications as they have show remarkable electrical and mechanical properties. Different methods are used for the synthesis of ceramic nanocomposites such as spray pyrolysis, polymer precursor route, sol-gel process template synthesis, etc. Examples of ceramic nanocomposites include Al_2O_3/SiO_2, Al_2O_3/TiO_2, Al_2O_3/CNT, $MgAl_2O_4/$ CNT, etc [79].

- **Metal Matrix Nanocomposite**

Metal matrix nanocomposites are composed of metal or also alloy as a matrix phase in which nanoparticles reinforcement is embedded. These metal/alloy nanocomposites have extraordinary physical, chemicals and mechanical properties. They are synthesized by various techniques such as spray pyrolysis, vapor techniques, rapid solidification, sol-gel methods, etc [80]. Examples of metal-matrix nanocomposites include $Fe-Cr/Al_2O_3$, Ni/Al_2O_3, Al/CNT and Mg/CNT, Fe/MgO.

- **Polymer Matrix Nanocomposite**

Polymer matrix nanocomposites composed of polymers as a matrix phase in which nanoadditives embedded as reinforced phase. These additive may be one dimensional such as nanotubes, two dimensional such as clay or three dimension such as spherical particles. Polyamide is a polymer in which carbon and glass fibers are embedded as reinforcement materials. Nano-fillers can be in many configurations and sizes, namely tube like, plate-like or 3 dimension particles. Polymers have poor electrical and mechanical properties which can be enhanced by the formation of nanocomposite. Polymeric matrix usually has weak interactions with filler material or in some cases; chemically bonding between matrix and nanofillers with unique anisotropic geometry will result in increased mechanical properties [81].

These polymeric nanocomposites can be synthesized by melt mixing, in situ polymerization, sol-gel process, template synthesis, etc. Vollenberg and Heikens produced nanocomposite by mixing of fillers and polymeric matrix such as by mixing polystyrene, polycarbonates and polypropylene with alumina nanoparticles (35 nm) as a filler. Properties of polymer nanocomposites depend on type of filler used, its size, rate of mixing of two phases, volume fraction of nanoparticles, morphology of filler material, etc. The nanofiller should be dispersed uniformly in polymer matrix; otherwise agglomeration will result in poor properties of nanocomposite [82].

1.7.2 Application of Polymeric Nanocomposites

Nanocomposites have broad range of applications in different fields due to their enhanced mechanical, electrical, optical and magnetic properties. In 1980s Toyota synthesized nylon 6/montmorillonite nanocomposite and used it for timing belt cover in their car model. It was the first polymer/clay nanocomposite with high mechanical properties [83]. As polymers have poor electrical conduction and fire resistance, so the addition of nanoclay as reinforcement in polymer can improve fire resistance of polymer by delaying of melting point and reduces air diffusion into polymer. These polymer/ clay nanocomposites have wide range of applications in vehicles, submarines and aeroplanes

to reduce fire risk [84]. Nguyen and Diaz have reported microwave absorption properties of polypyrrole nanocomposite with tin oxide, iron oxide and titanium oxide nanofillers [78]. Polymer nanocomposites have high range of scratch resistance due to high hardness and Young's modulus, such as PP/clays nanocomposites. Rapoport, et al have reported lubricating properties of tungsten sulphide nanocomposite with epoxy: polyacetal to reduce coefficient of friction between steel discs [85]. Conjugated polymeric nanocomposite with nanofiller has been reported as a gas and biosensors. Polymeric based nanocomposites have also been used in solar cell to form large flexible solar panels [78].

1.7.3 Nanocomposite Fabrication Methods

The fabrication of nanocomposites requires uniform dispersion of nanoparticles in the polymer matrix which poses a major problem because nanoparticles usually form aggregate, which limits their dispersion in polymer matrix [86]. Generally, there are three approaches through which nanoparticles can be uniformly dispersed. The first approach is direct mixing of nanoparticles and polymer matrix, the second approach is solution blending, and the third approach is blending of nanoparticles with pre-made polymer.

1.7.3.1   Melt Intercalation Method

Melt intercalation method is used at industrial scale to synthesize nanocomposites.
It involves mixing of nanoparticles or nanoclay and polymer matrix at molten temperature to anneal the mixture. This method involves melting of polymer into a viscous liquid followed by addition of nanofillers at high shear rate and high temperature diffusion. Finally the nanocomposite can be obtained by compression molding [74]. One of the disadvantages of melt mixing is risk of agglomeration of nanofiller in polymer matrix which can be overcome by another method known as solution blending.

1.7.3.2   Solution Blending

This is a widely used technique to form nanocomposites and involves dispersion of nanoparticles along with polymer matrix in a suitable solvent. Polymer is first dissolved in a suitable solvent and later mixed with nanofiller at room temperature. The mixture is poured into a Petri dish and solvent is allowed to evaporate.   The nanocomposite is obtained as a film. This is the simplest method employed at laboratory scale but difficult to be used at industrial level due to requirement of large quantity of solvent [87].

1.7.3.3   In-Situ Polymerization

In in-situ polymerization method, nanofillers are first dispersed in a monomer solution followed by polymerization. In this method, polymer matrix grafts over the nanoparticles surface [88]. Nanoparticles or nanofillers swell in monomer solution because of seepage of low molecular weight monomer solution between nanoparticle layers. The resulting solution is polymerized by using radiations, heat, or by organic initiator and the monomer is polymerized in interlayer to form intercalated nanocomposites. Different polymer nanocomposites have been synthesized by in-situ polymerization such as polypyrrole/silver nanocomposite, nanotube/polypyrrole nanocomposite, and multi-walled carbon nanotube/polypyrrole nanocomposite [89].

1.7.4 Nanocomposites of Polypyrrole-Literature Survey

Polypyrrole has wide range of applications and its properties can be enhanced by addition of nanofillers to form nanocomposites.

Jyoti Srivastava, et al[90] synthesized silver/polypyrrole/polyvinylalcohol nanocomposite by in-situ polymerization method with different silver weight percentage i.e. 0.5-10 %. Both thick and thin films of Ag/Polypyrrole/PVA were synthesized. UV-Visible and FTIR has confirmed Ag/PPy nanocomposite formation in a PVA matrix. Synthesized nanocomposite was used for EMI shielding (electro magnetic impedence). Maximum shielding was observed with 10 wt % loading of silver nanoparticles.

Panagiotis Dallas and Dimitrios Niarchos [91] synthesized a polypyrrole/silver nanocomposite by in-situ polymerization using Fe(III) as an oxidant while SDS or CTAB was used as surfactant. Size and different morphologies of polypyrrole were obtained depending on surfactant used. The nanocomposite was characterized by XRD,FTIR, and thermo gravimetric analysis. Polypyrrole with the size range of 200-300 nm was obtained and EMI showed different morphologies of polypyrrole depending on surfactant .

Morteza Farkhondekalam Ghadim et al synthesized [92] PPy-Ag nanocomposite by using surface modified silver nanoparticles. Polymerization with pyrrole monomer occurred with 1:1:1 molar ratio of monomer: initiator: silver nanoparticle. Nanocomposites of varied weight percent of Ag nanoparticles were formed and were characterized by XRD, FTIR, SEM, TEM, TGA and four point resistivity meters. TEM analysis showed semi spherical nanoparticles disperse in PPy with 40-70 nm particle size.

Ruma Gupta, et al [93] synthesized polypyrrole/Ag nanocomposite by photodynamic polymerization of pyrrole and electrodeposition of silver nanocubes. X-ray diffraction and scanning electron microscopy were used for nanocomposite characterization. It was reported after electron paramagnetic resonance that increased silver nanoparticles deposition increases carrier density and enhances electrical conductivity. Electrocatalytic performance of nanocomposite was determined for hydrogen reduction.

V.T. Bhugul, et al[94] used sol gel process for the synthesis of ZnO nanoparticles doped with 6 % aluminium. In-situ polymerization was used to synthesize polypyrrole-ZnO-Al doped nanocomposite. Chemical interaction between PPy and ZnO nanoparticles (Al doped) was confirmed by FTIR spectrum which showed shifting of peaks toward lower wave number along with broadening of peaks. TGA and DSC analysis confirmed high thermal stability of nanocomposites. Amorphous nature of polypyrrole-ZnO-Al doped nanocomposite was confirmed by XRD analysis.

Pawan K. Khanna et al [95] synthesized polypyrrole /Se and polypyrrole/CdSe nanocomposites by in situ polymerization using Selenium oxide and cadmium selenide as an internal oxidant. They used chemical as well as microwave methods for the formation of nanocomposite.. XRD confirmed the formation of polypyrrole/Se and polypyrrole/CdSe nanocomposite. Heavy metal removal applications of these nanocomposites were studied.

1.8 Motivation

Polypyrrole has gained considerable interest in the scientific community because of its high conductive and good thermal behavior. However, due to large intramolecular interactions between polymer chain and presence of bulky ring in its structure, the polymer is always obtain as a black brittle powder with lack of essential mechanical, processibility and film forming properties. On the other hand, SIS or polystyrene-blocked-polyisoprene-blocked-polystyrene is a thermoplastic insulating polymer with high mechanical properties. **In this research work, the synergistic assemblage of polypyrrole with SIS copolymer is studied and Ag-Pd/PPy-blend-SIS nanocomposite is synthesized to investigate the effect of Ag-Pd bimetallic nanofillers on the mechanical and electrical properties of blends .A novel method for the synthesis of Ag-Pd bimetallic nanoparticle using Camellia sinensis(Green Tea) extract is investigated. The main objective of research work is to provide greater level of processability to brittle, infusible polypyrrole and enhance its mechanical properties**.

CHAPTER 2
EXPERIMENTAL

2.1   Materials

The precursors used in the research work include: Palladium chloride ($PdCl_2$) was purchased from Merck. Silver nitrate ($AgNO_3$) was purchased from Sigma Aldrich. Iron (III) chloride anhydrous, functioning as the oxidant, and was obtained from Sigma Aldrich. Pyrrole was purchased from Fluka BioChemika and was distilled before use. Methanol and acetone were used in washing process, and were purchased from Fluka. Deionized water was purchased from Vitro diagnostics laboratory Islamabad, SIS triblock was purchased from Sigma Aldrich.

2.2   Green Chemistry Methods for the Synthesis of Nanoparticles

 Synthesis of nanoparticles by chemical methods has some associated disadvantages, such as toxicity of chemicals, expensive chemicals, long reflux time and toxic byproducts are obtained at the end of reaction. Green chemistry methods have recently gained due to their low cost and eco friendliness. In present research work, green tea extract *(Camellia sinensis)* was used for synthesis of bimetallic nanoparticles, which is explained in the next section.

2.2.1 Composition of *Camellia sinensis(Green Tea)*

Use of *Camellia sinensis* extract for reduction of nanoparticles has gained considerable interest recently. Green tea leaves are rich in polyphenols, commonly known as catechins with almost 30 % content. It also contains, 15 %, proteins, 4 % amino acid, 7 % carbohydrates, 7 % lipids and vitamin C and E. Polyphenols exhibit high antioxidant potential to reduce metal ions into nanoparticles which are further stabilized and capped

by proteins, lipids or amino acid, thereby eliminating the need of using external surfactant and capping agent for nanoparticle stabilization [96].   Green tea extract is rich in six major phenolic catechins, including (−) epicatechin (EC), (−) epicatechin-3-gallate (ECG), (−) epigallocatechin (EGC), (−) epigallocatechin-3-gallate (EGCG), (+) catechin, and (+) gallocatechin (GC) as shown in Figure 2.1 [96]. Among these catechins (−) epigallocatechin-3-gallate (EGCG) is most important because it represents 59 % catechin content, while EGC exhibits almost 19 %, ECG 13.96 % and EC at approximately 6.4 % of total phenolic catechin content. Other phenolic catechins are also important component of green tea such as chlorogenic acid caffeic acid and flavonols, such as kaempferol, myricetin and quercetin [97].
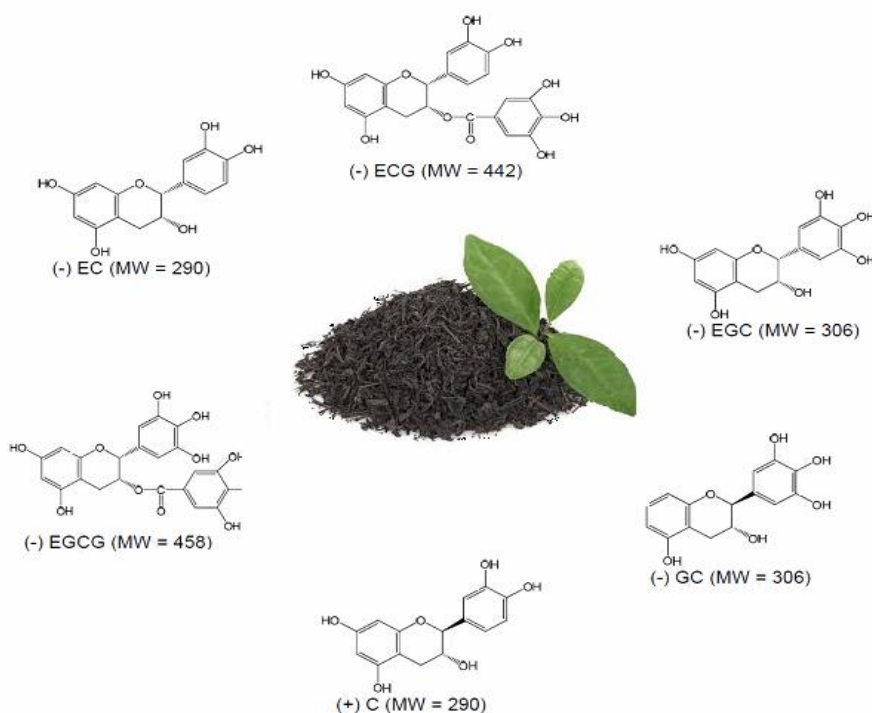
Figure 2.1: Different Polyphenolic catechins present in a Green Tea

2.2.2   Preparation of Green Tea Extract

Firstly, the green tea extract was prepared by taking 1.0 g of green tea leaves in 250 mL conical flask with 100 ml deionized water. Next, the mixture was boiled for 15 minutes at 60 °C and was filtered to get extract

2.2.3 Preparation of Ag-Pd Bimetallic Nanoparticles

Ag-Pd bimetallic nanoparticles were prepared by adding 50 mL of freshly prepared extract of *Camellia sinensis* in continuously stirred solution (100 mL)of 15mM $AgNO_3$ (0.2g/100 mL), heated at 45 °C for 15 minutes. The color of silver nitrate solution changed from colorless to dark brown indicating formation of silver nanoparticles. In the next step, 50 mL of 15mM aqueous solution of $PdCl_2$ (0.27g/100 mL deionized water) was added to a solution of Ag nanoparticles under stirring at ambient temperature and the color of solution changed to dark green. Stirring was continued for 1 hour. Then the resulting bimetallic nanoparticles were centrifuged at 8000 rpm and washed three times with deionized water. Finally, the black powder was dried at 85 °C for 8 hours in heating oven. Percentage yield of reaction was 89 %. Synthesis scheme of Ag-Pd bimetallic nanoparticles by green tea method is shown in Figure 2.2.

Figure 2.2: Preparation of Extract and Synthesis of Ag-Pd Bimetallic Nanoparticles

2.3   Synthesis of Polypyrrole

Polypyrrole was synthesized by chemical polymerization, using anhydrous ferric chloride $FeCl_3$ as an oxidant. For this purpose 2.38 g of $FeCl_3$ was added into 50 mL chloroform and stirred for 15 minutes at 25 °C. Pyrrole was distilled before use in order to remove inhibitors. Then, 10 mL pyrrole was added drop-wise into the iron chloride solution with continuously stirring while temperature was maintained at 30 °C. The color of solution turned black right after the addition of first drop of pyrrole indicating the formation of polypyrrole. Polymerization process was continued for 3 hours under moderate stirring. Black precipitates of polypyrrole were filtered followed by washing with methanol and distilled water in order to remove color of ferric chloride and finally with acetone. The black polypyrrole powder was dried under vacuum at 40 °C for 8 hours.
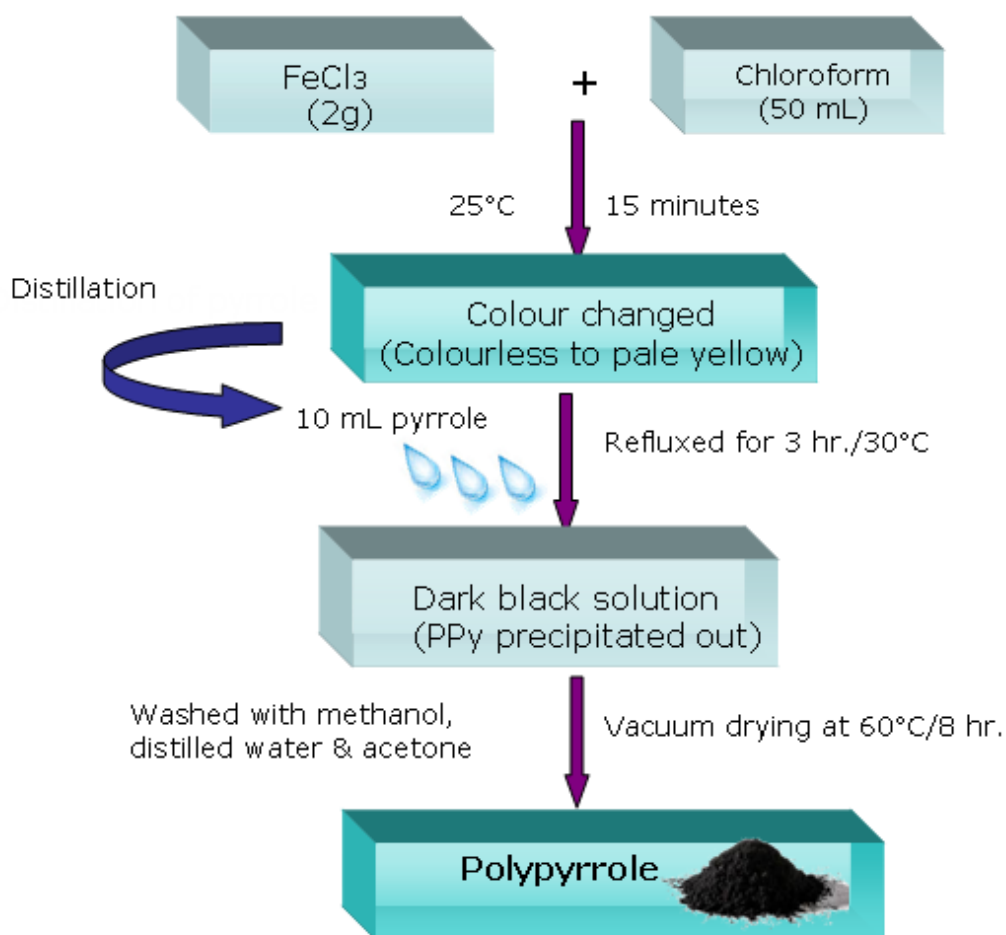
Figure 2.3: Synthesis Scheme of Polypyrrole

2.4   Preparation of PPy /SIS Blends

Blends of polypyrrole/SIS copolymer were prepared by mechanical mixing of polypyrrole with SIS copolymer, in different molar ratios. Polypyrrole was dispersed in varying weight % in SIS copolymer by using chloroform as solvent. Stirring was continued for 24 hours at room temperature and after complete dispersion the mixture was poured into a Teflon Petri dish and left overnight for evaporation. Films of 0,6,10,15, and 20 weight % were made by this method. Each film was dried in vacuum oven for 24 hours at 45°C. 20 wt. % PPy-SIS blends shows selective agglomeration of

polypyrrole particles with each other instead of with SIS copolymer .PPy/SIS blends are shown in Table 2.1.

Table 2.1: Polypyrrole/SIS blends with different wt. % of PPy.

Amount of SIS	Amount of PPy	PPy/SIS Blends
1g SIS	0g PPy	Pure SIS film
0.94g SIS	0.06 g PPy	6 wt.%PPy/SIS blend
0.90g SIS	0.1g PPy	10 wt.% PPy/SIS blend
0.85g SIS	0.15g ppy	15 wt.% PPy/SIS blend

0 wt. % PPy

6 wt. % PPy
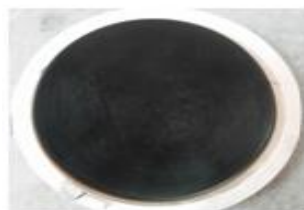
10 wt.% PPy
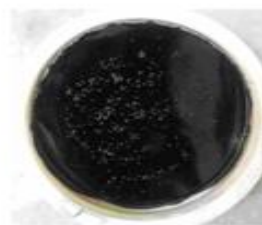
15 wt.% PPy

Figure 2.4: Films of Polypyrrole/SIS Blends with Different Weight %

2.5   Nanocomposite Formation of Ag-Pd/PPy-SIS Copolymer

Nanocomposites of Ag-Pd/ PPy-blend-SIS were prepared by adding bimetallic nanoparticles as reinforcement to the PPy-blend-SIS. In this case PPy-blend-SIS matrix phase properties are enhanced by bimetallic reinforcement. The composition of nanocomposites varied between 1-5 % by weight of Ag-Pd nanoparticles. Bimetallic nanoparticles were dispersed in matrix by solution blending, using chloroform as solvent. . Stirring was continued for 24 hours at room temperature. After a complete dispersion, the mixture was poured into a Teflon petri dish overnight to evaporate solvent .Films of 1,3 and 5 weight % nanoparticles were made and each film was dried in vacuum oven for 24 hours at 45 °C. Different .blends are shown in Table 2.2

Table 2.2: Ag-Pd/SIS-PPy Nanocomposites with Diff. Weight %

Amount of SIS	Amount of PPy	Amount of Ag–Pd NPs	Ag–Pd/15wt.%PPy-SIS Nanocomposites
0.85g SIS	0.15g PPy	0.01g Ag–Pd Nanoparticles	1 wt.%Ag–Pd/PPy-SIS Nanocomposite
0.85g SIS	0.15g PPy	0.03g Ag–Pd Nanoparticles	3 wt.% Ag–Pd/PPy-SIS Nanocomposite
0.85g SIS	0.15g PPy	0.05g Ag–Pd Nanoparticles	5 wt.% Ag–Pd/PPy-SIS Nanocomposite

2.6   Characterization Techniques

2.6.1   X-RAY Diffractrometer

X-ray diffraction is a non destructive characterization technique to provide structural, phase, size, crystallinity information of a material. X-rays are electromagnetic radiation having energy in the range of 100 eV-100 keV. X-rays with the wave length of 0.1 angstroms are used for diffraction, since the wavelength is comparable to the inter-layer spacing in a crystal lattice. These are known as short wavelength X-rays or hard X-rays [98]. These X-rays have high energy and can penetrate into, material to provide structural information of atoms or molecules, i.e. structural arrangement. X-ray diffraction is based on Bragg's law which explains constructive interference of monochromatic radiations diffracted by crystalline material. These monochromatic radiations are generated in a cathode ray tube are directed toward sample by using collimator. The X-rays on interaction with the sample, produces diffracted rays which on constructive interference are explained by the Bragg's law:

$$n\lambda = 2d\sin\theta$$

Where n is an integer, λ represents wavelength, d is interspacing between two crystalline plane and θ is angle of diffraction. This law shows relationship between wavelength of X-rays to the angle of diffraction and lattice spacing between crystalline planes. These X-rays are then detected and counted [99].
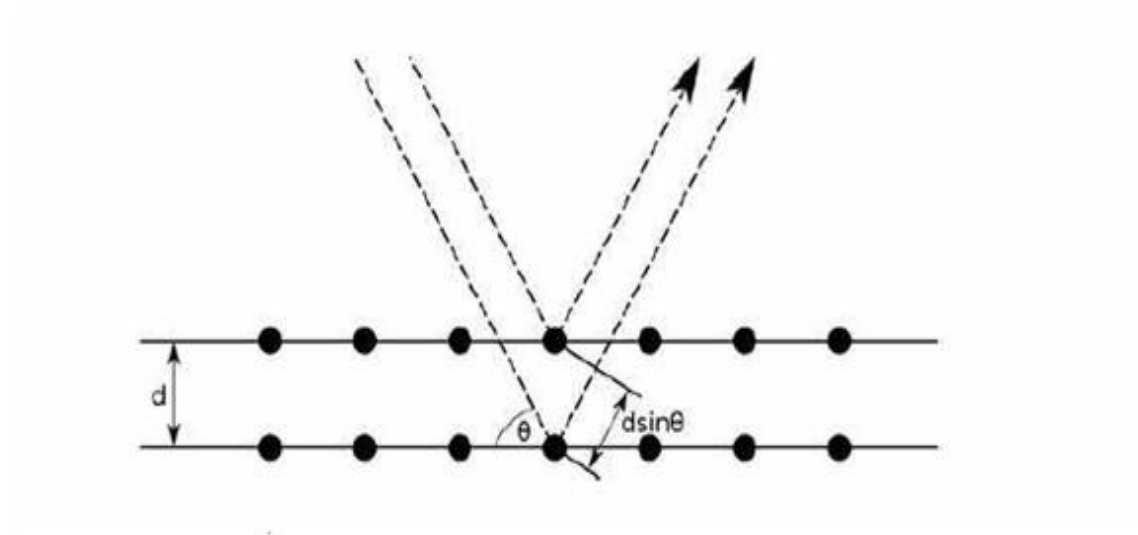
Figure 2.5: X-rays Diffraction from Crystalline Planes

Three important components of X-ray diffractrometer are: a X-ray tube, a sample holder, and X-ray detector.

The X-ray tube consists of rotating Copper anode X-ray source and negatively charged metal filament acting as cathode. X-rays are generated by heating negatively charged filament in a cathode ray tube to produce electrons. These electrons are then accelerated toward target by applying high voltage current between cathode and anode. These electrons bombarded the anode (target material) .If they have sufficient energy to penetrate into material it will knockout inner shell electron, creating holes. Subsequently, electrons from high energy shell will jump to inner shell releasing energy in the form of X-rays producing X-ray spectra .These X-ray spectra composed of $K\alpha$ and K_β lines. $K\alpha$ consist of Shorter wavelength $K_{\alpha1}$ and longer wavelength $K_{\alpha2}$. Mostly copper is used as a target material for single crystal diffraction with Cu $K\alpha$ radiations with 1.5418 Å. Intensity of diffracted X-rays is recorded
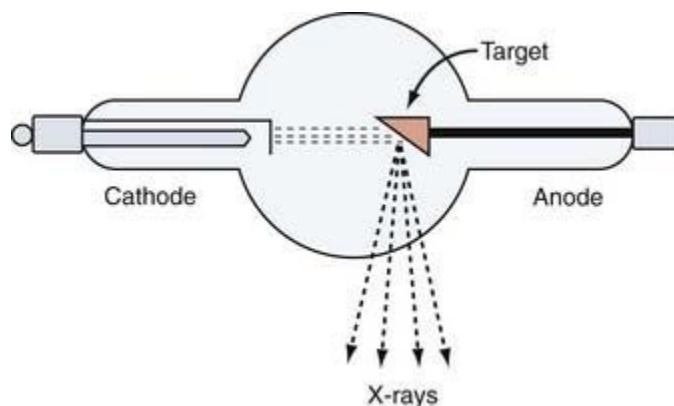
Figure 2.6: X-ray Tube

Constructive interference occurs when Bragg's law is satisfied. These X-ray signals are detected and processed by a CCD (charged-coupled device) camera detector and converted into count rate, which is then output to a printer [100].

The XRD pattern obtain is a characteristic of a material under examination and it gives information regarding: (1) size and shape of unit cell (2) Quantitative analysis is determined by relative peaks intensity.

For determination of unit cell parameters from peaks positions indexing is performed by assigning hkl values to each peak. Indexing is the first step in analysis of XRD data which gives information about crystal system. It is a complicated process. For simple structures like a cubic crystal, manual indexing is performed but auto indexing is used for complex structures. Steps involved in indexing of samples are : (1) Peak identification, (2) determination of $\sin^2\theta$, (3) Calculation of $\sin^2\theta/\sin^2\theta_{min}$ ratio and multiplying it with appropriate integers,(4) Selecting result from step (3) to obtain $h^2+k^2+l^2$ value.(5) Identification of Bravais lattice by comparing result with $h^2+k^2+l^2$ sequence, e.g. (6) Calculation of Lattice Parameters .These steps are outlined in Table 2.3 [101]

Table 2.3: Indexing of XRD Data

Peak No.	2θ	$\sin^2\theta$	$1\times\dfrac{\sin^2\theta}{\sin^2\theta_{min}}$	$2\times\dfrac{\sin^2\theta}{\sin^2\theta_{min}}$	$3\times\dfrac{\sin^2\theta}{\sin^2\theta_{min}}$	$h^2+k^2+l^2$	hkl	a (Å)
1	38.43	0.1083	1.000	2.000	3.000	3	111	4.0538
2	44.67	0.1444	1.333	2.667	4.000	4	200	4.0539
3	65.02	0.2888	2.667	5.333	8.000	8	220	4.0538
4	78.13	0.3972	3.667	7.333	11.000	11	311	4.0538
5	82.33	0.4333	4.000	8.000	12.000	12	222	4.0538
6	98.93	0.5776	5.333	10.665	15.998	16	400	4.0541
7	111.83	0.6859	6.333	12.665	18.998	19	331	4.0540
8	116.36	0.7220	6.666	13.331	19.997	20	420	4.0541

Average lattice parameter is 4.0539 Å

Particle size from XRD data is obtained by using Debye-Scherrer's formula, given as:

$$D= K\lambda/ \beta \, Cos\theta$$

Where "λ" is wavelength of incident X-rays, "β" is full width at half maximum obtained fro peak broadning, and "θ" is Bragg's angle and K is a shape factor, whose value is 0.8-0.9. By putting all these in given formula, particle size can be easily calculated [102].

2.6.2   Scanning Electron Microscopy Coupled with EDX

Scanning electron microscope is an imaging technique that gives surface morphological information including morphology and surface topology by focusing high energy beam of electron over the specimen. Electron beam can give image with better resolution as compare to optical light and generate variety of signals while interaction with sample. For conventional SEM technique, approximately 1 cm to 5 microns in width area can be imaged [103].

 "Accelerated electrons in a SEM with high kinetic energy are targeted on a specimen, and on interaction with the sample, energy is dissipated in the form of secondary electrons, backscattered electrons, diffracted backscattered electrons, visible light (cathodoluminescence), heat and photon. These signals are further processed by detector

to form image of sample on cathode ray screen. Secondary electrons and BSE give useful information about topography and contrast in composition respectively." [103].

Important components of scanning electron microscopy are electronic console and electron column. Electronic console consist of switches to control filament current, voltage, magnification, contrast and brightness. Electron beam is generated in electron column under vacuum conditions ($5x10^{-5}$ Torr pressure) and focused to a selected area of specimen by electromagnetic scanning coils. Lower portion of column is known as specimen chamber. Inside the specimen chamber secondary electron detector is located above the sample stage [104]. Sample stage is controlled by gonimeter. Important components of electron column are: electronic gun, condenser lenses, aperture, scanning system and specimen chamber. Electronic gun is located at the top of electron column. Electron beam is generated by tungsten filament heated at ~ 2700K in an electron column and accelerated toward anode by applying 200V to 3 kV. After passing through anode the electron beam is converge by two condenser lens [104]. Apertures in electron column reduce and exclude extraneous electrons in the lenses. The final lens aperture determines the spot size of the beam at the specimen as decreasing the spot size will increase the resolution and depth of field. At the end of objective lens, a stigmator is located to decrease aberrations of electron beam. The specimen chamber is located at the lower portion of the column. Secondary electrons signals coming from specimen are directed toward detector by positive charge. SEM operates under high vacuum because the temperature of filament can be easily reached up to 2700 K under vacuum condition, secondly the column optics can work properly in dust free environment and thirdly, the electron beam can reach the specimen without being interrupted by dust particles in vacuum conditions [104].
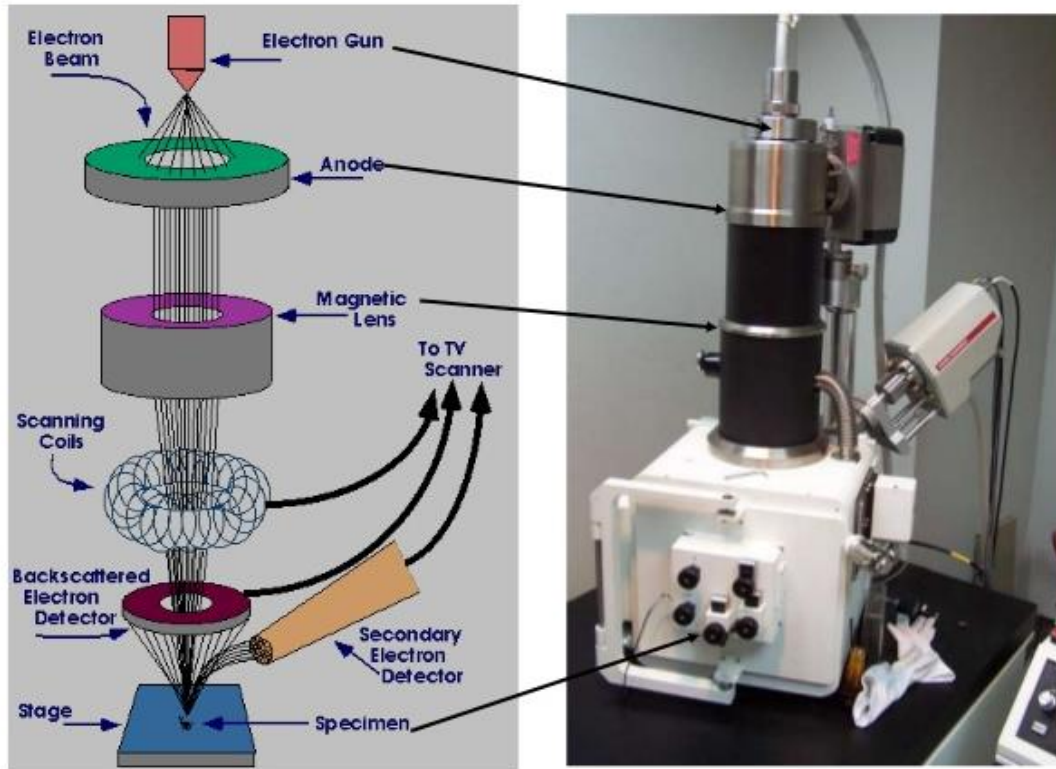
Fig. 2.7: Schematic Diagram of SEM

When electron beam strikes with specimen it generates variety of signals as shown in Figure 2.8 [105]. Surface morphology and visual information is provided by two types of signals, i.e. those coming from secondary electron and backscattered electrons. Secondary electrons are generated due to inelastic collision with the sample and have energy of less than 50 eV; they give information about surface of specimen. Backscattered electrons are generated due to elastic collision with the nuclei of the sample atoms and penetrate deeper into the specimen to give topographical contrast and atomic number contrast. Density variations in a sample can be detected by using BSE detector. Along with these signals, X-ray signals can also be generated on interaction with the sample (EDX analysis) give information about surface composition [105].
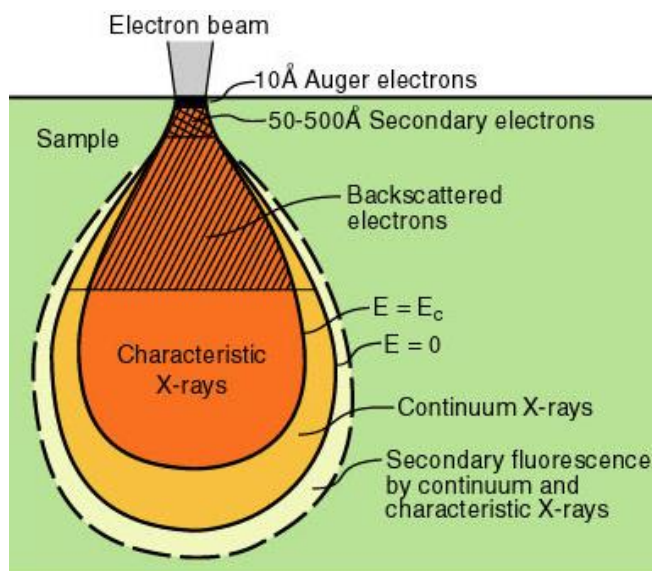
Figure 2.8: Different Signals Generated by Electron Beam-Specimen Interaction

EDX systems are coupled with scanning electron microscopy (SEM) and TEM (transmission electron microscopy). Energy dispersive X-ray spectroscopy is used for elemental analysis of sample by making use of X-ray spectrum emitted by solid sample. It involves interaction of an electron beam with the specimen and as a result of interaction of electron beam and sample; varieties of signals are generated along with characteristic X-rays of different elements. These characteristic X-rays are separated by energy dispersive detector which is further analyzed by EDX system software to determine the abundance of specific element [106]. EDX can be used to create elemental map over a broader raster area. It can detect element from Be_4 to U_{92}.

EDX has X-ray sensitive detectors working under a nitrogen atmosphere and software to analyze spectra. Detector is present in a sample chamber at the end of long arm which is also equipped with nitrogen cooling system .Mostly detectors that operate at low voltage with high sensitivity are made up of Si(Li) crystals. Recently detectors with high count rate known as "silicon drift detector" are now used that can work without nitrogen cooling system [106].

Energy of in-coming electrons is absorbed by the crystal in an EDX detector by ionization. As a result free electrons are generated inside the crystal making it conductive and producing an electric charge bias. The absorption of X-ray thus converts individual

characteristic X-rays into electric signals. EDX data is obtained as energy peaks correspond to each element in a sample, and spectrum is obtained between X-ray count and energy in keV, giving true composition of sample under analysis. Mostly these energy peaks are narrow and sometime many elements yield multiple peaks. Elements that are present in low abundance generate peaks with low intensity and can not be resolved easily. EDX is non-destructive technique and can be performed with little or no sample preparation.

2.6.3   Fourier Transform Infrared Spectroscopy

Fourier transform infrared spectroscopy is the study of vibration of a molecule as a result of absorption of electromagnetic radiation in infrared region (400-4000 cm^{-1}). In FTIR, the IR spectrum is split in to two regions:

- 4000-1000 cm^{-1} known as the ***functional group region***, and
- < 1000 cm^{-1} known as the ***fingerprint region***

FTIR analysis is used for identification of compounds as it provides a fingerprint pattern for functional groups. Functional groups in a molecule give absorption band in a specific region of IR which helps in the structural analysis of a sample. When infrared radiation targeted on a sample some of the radiation is transmitted while those radiations which cause change in dipole moment will be absorbed by the sample. As a result, we see different bands in the FTIR spectrum corresponding to symmetrical, asymmetrical, out-of plane and in-plane bending [107] as shown in Figure 2.9.
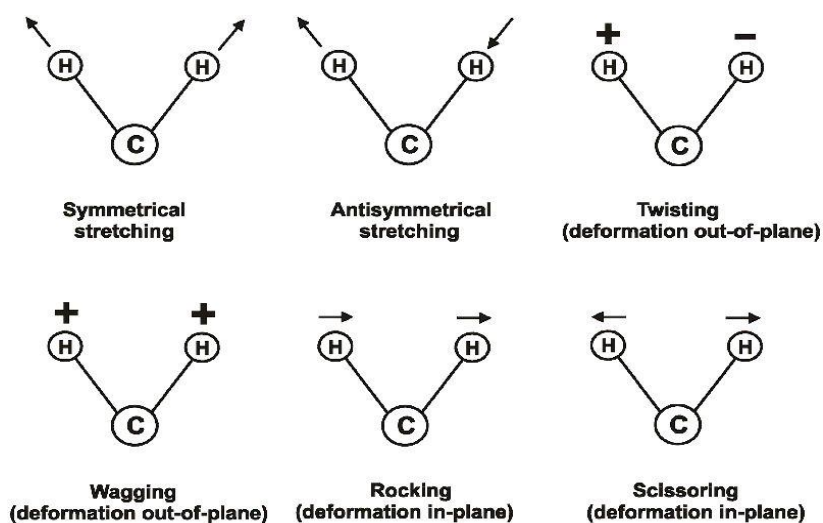
Figure 2.9: Different types Stretching and Bending Vibrations

Stretching frequencies can be calculated by Hooke's law according to which two bonded atoms are treated as simple harmonic oscillator. The equation given by Hooke's law shows relation between frequencies, atomic masses of two bonded atoms and force constant of bond between two atoms is given as:

$$\text{Stretching frequency} = \bar{\nu} = \frac{1}{2\pi c} \left[f \frac{m_A + m_B}{m_A m_B} \right]^{1/2}$$

Where **v** is the vibration frequency in cm^{-1}, **c** is velocity of light in cm/s, **f** is force constant of bond in dyne/cm approximately equal to 5×10^5 dyne/cm for single bond while it is two and three times for double and triple bond respectively, $m_A m_B$ are masses of atom A and B respectively [107].

The important components in FTIR instrumentation are source, monochromator, sample holder, detector. Infrared radiations after generation at a source passed through single wavelength selector, monochromator and than to interferometer where spectral encoding occurs. After wards, IR radiation beam of single wavelength passed through the sample where some radiations are transmitted while some radiations of specific frequencies are

absorbed and detected by the detector which is designed to measure specific interferogram signals .These signals then undergo Fourier transformation by the computer which gives spectrum in the form of band as a function of wave number and [108].

2.6.4 Two Point Probe Conductivity Measurements

Electrical conductivity is an important property of a material and two important techniques are used to measure electrical conductivity. These are: Two point probe and four point probe methods. Four point probe is used to measure resistivity of low resistance materials while two point probe is used for high resistance materials. It is simple and less expensive tool as compare to four point probe method [109].

Two point probe measures electrical conductivity according to Ohm's law that deals with the voltage apply and current flow through the conductor and is stated as:

"The voltage or potential difference across conductor is directly proportional to current flow through it"

Ohm's Law is given by:

$$V \alpha I$$

$$V = RI \quad or$$

$$R = V/I$$
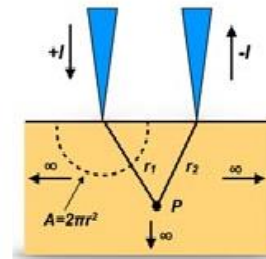
Where V is the potential difference applied and I is current flow while R is resistance (constant of proportionality).Conductance is inverse of resistance and its units are Siemens.

$$C = 1/R \ (S)$$

In two point probe method, alternating current is applied between two point tip and potential difference (V) across the two points is measured to find the resistance of a

specimen. Two point probe method conductometer is composed of osmium or tungsten carbide probe tips where each probe tip is mounted at the end of separate arm. There are pivots on kinematics bearing system that control the motion of probe tip when they are in contact with sample. The two probe tips are separated at a distance less than a 20 μm. In order to measure resistance of a sample, these two probe tips are lowered onto the sample in a controlled manner [110]. For measuring electrical resistivity of sample, electrodes are fabricated on sample by applying silver conducting paste at the same surface of sample [111]. Two probe electrical resistivity is measured at room temperature by using high resistance meter Agilent 4339 B shown in Figure 2.10, which can measure surface resistivity up to 7.0×10^{17} Ohm-cm. Surface resistivity of a sample is measured by using formula:

$$\rho_s = \frac{V \times A}{I \times t} = \frac{R_s \times A}{t}$$

Where R_s is surface resistivity of sample, A is area of cross-section of a sample and t is the distance between two electrodes probe on the sample. From resistivity value conductivity of a sample can be measured since conductivity is inverse of resistivity. It can be written as:

$$\sigma = 1/\rho$$

Where σ is conductivity in and ρ is resistivity of a sample in "ohm metre" ($\Omega \cdot$m)
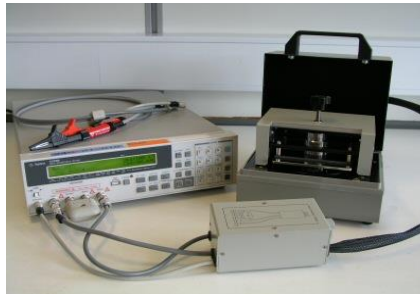
Figure 2.10: High Voltage Resistometer

2.6.5 Mechanical Testing

Tensile strength refers to the stress a material can withstand before breaking. It Tensile strength is measured by using mechanical testing machine. Where the basic principle of mechanical testing machine is: [112]

"Subjecting a test specimen to a continuously increasing strain to a fracture point, to determine tensile strength, percentage elongation and ductility of material by percentage reduction of area."

Mechanical testing is performed according to ASTEM standards to find resistance of material against applied force. Information related to the strength, stiffness, and ductility of a material can be obtained from a mechanical testing. In this method, the specimen is mounted onto a testing machine in a controlled manner and deformed by applying constant force. The tensile testing machine consist of one static grip and one wedge or movable grip that moves with constant velocity to elongate the specimen until its fracture point. Elongation of specimen is measured by strain gauge or extensometer. The resulting output is obtained as force vs. displacement curve and is then converted to Stress vs. percentage strain curve.Schematic diagram is given in Figure 2.11 [112].
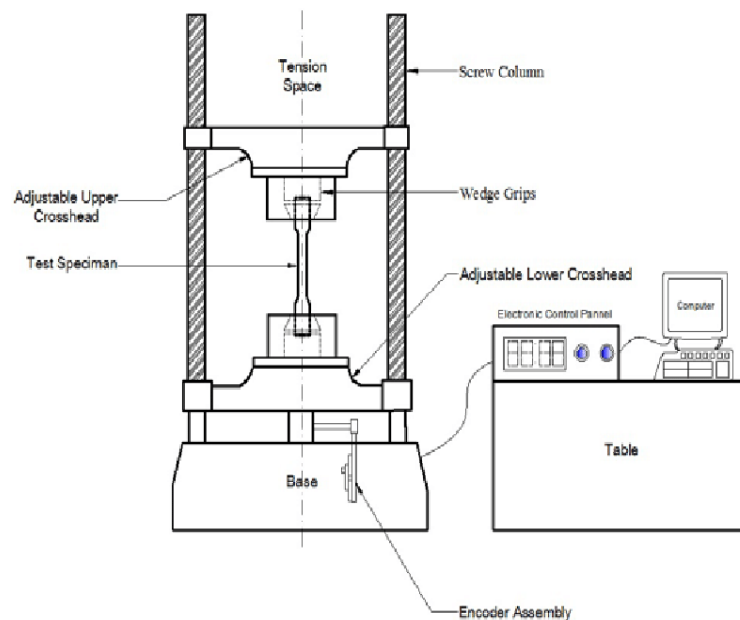
Figure 2.11: Tensile Testing Machine

Different tensile properties can be calculated from stress vs. % strain curve such as Young's modulus, stress at fracture point and % strain at fracture point, percent total elongation etc.

ASTEM D882 standard is used to measure the tensile strength of plastics in the form of thin sheets, including films which are less than 1 mm in thickness [113].

Before starting the test, gauge length is measured. I.e. according to ASTEM D882 gauge length selected for polymer film is 20 mm. Area of cross section is calculated from width and thickness of specimen for each sample, i.e 10mm and 0.34mm respectively. The sample is then clamped on machine and remote connection is established. One end of specimen is fixed in a static grip while the other end is pulled continuously with constant velocity until the sample fractures. After establishing the connection live image appears on computer screen followed by setting the test parameters, starting the test and saving the data. The test is performed until sample fractures. The details appear as a graph between force and displacement which is later converted to stress and strain.

 Stress is defined as the force applied per unit area to produce deformation in a test specimen.

Stress is a ratio of applied load to the original cross-sectional area.

$$\sigma = F/ W \times d \qquad\qquad\qquad \text{eq. (1)}$$

Strain is the ratio of the change in length over original length of a specimen. It is expressed as a dimensionless ratio.

$$\textbf{Strain = Change in length/original length}$$

$$\varepsilon = \Delta L/L \qquad\qquad\qquad \text{eq.(2)}$$

The shape and dimensions of the specimens are exhibited in Figure 2.12 and Table 2.2. At least five samples we used for each nanocomposite.

Table 2.4: Dimensions of Tensile Test Specimen

Symbol, Definition	Dimensions of Specimen (mm)
W, Width of narrow section	10
T, Thickness of the specimen	0.34
D, Distance between grips	20
L, Total length of specimen	40

Young's modulus: Young's modulus is the ratio of stress to strain below the proportional limit of a material, calculated by drawing a tangent to first deformation point and measuring the slope between Stress-strain curve.

Young's modulus=Stress (σ)/Strain (ε)   **eq. (3)**
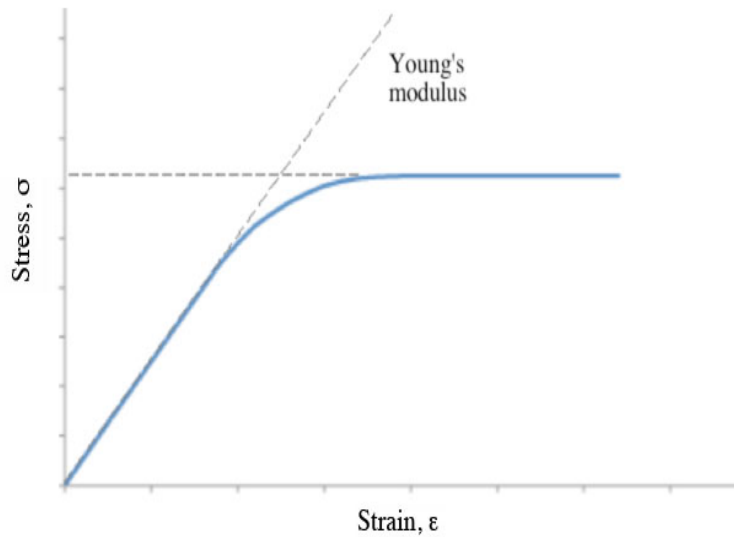
Figure 2.12: Calculation of Young's modulus from stress-strain curve

Proportional Limit: Point on a curve where stress and strain remains proportional is known as proportional limit point. It is represented by point "**P**" in a Figure 2.13.

Elastic Limit: It is that limiting value of stress up to which material remains elastic. It is represented by point "**E**" in a diagram.

Ultimate Stress Point: It is the highest stress borne by the film before it breaks. It is represented by "**U**" in a graph.

Breaking Stress : It is that point in a curve where a strength of material breaks. It is represented by "**B**" in a graph.
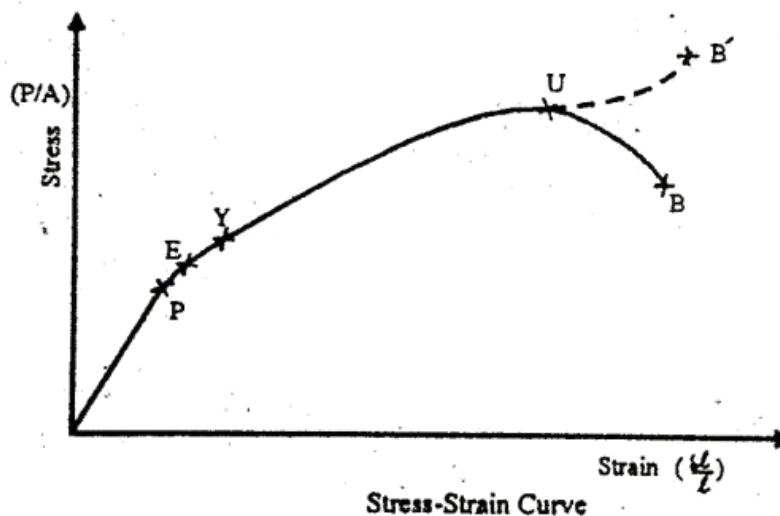
Figure 2.13: Different Points on Stress/Strain Curve

- **Determination Of Strength of Material by Stress-Strain curve**

Stress of a material is determined by area under the stress vs. strain curve. Brittle material has little strain with high stress and area under the stress vs. strain curve decreases with increase in strength of material. A flexible material has high strain with less stress and has increased area under the stress vs. strain curve. Material A in a curve is more brittle

as compare to B and C while curve D represents highly flexible material with high strain and less stress as shown in Figure 2.14.
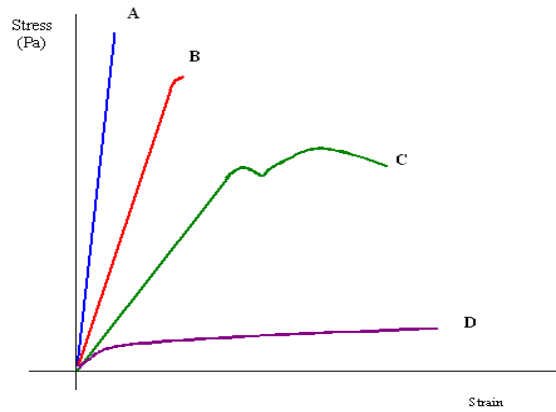
Figure 2.14: Reduction in area under the curve with increase in strength

CHAPTER 3

RESULTS AND DISCUSSION

3.1 Synthesis and Characterization of Ag-Pd bimetallic nanoparticles

3.1.1   Synthesis of Ag-Pd bimetallic nanoparticles

Ag-Pd bimetallic nanoparticles were synthesized by green chemistry approach using *Camellia sinensis* extract as a reducing agent. Green tea extract is in rich of polyphenolic catechins, carbohydrates, proteins and vitamins; they behave as reducing as well as capping agent. For the synthesis of Ag-Pd bimetallic nanoparticles, green tea extract was obtained by boiling green tea leaves followed by filtration. Then $AgNO_3$ was added into extract and mixture was heated at 45 °C for 15 minutes followed by addition of $PdCl_2$ solution at ambient temperature with constant stirring. The obtained nanoparticles were centrifuged and dried at 85 °C for 8 hours. Formation of nanoparticles was confirmed by XRD, FTIR and SEM analysis.

3.1.2   X-ray Diffraction Analysis of Ag-Pd Nanoparticles

The crystalline structure and synthesis of bimetallic nanoparticles was confirmed by X-ray analysis. For this purpose Rigaku X-ray diffractrometer was used, with CuK_α radiation source having wavelength (λ) equal to 0.154 nm equipped with graphite monochromator in a 2θ range of 5°-80° with 0.05 step at a time count of 1 second. All the diffraction analysis was done at room temperature under constant conditions.
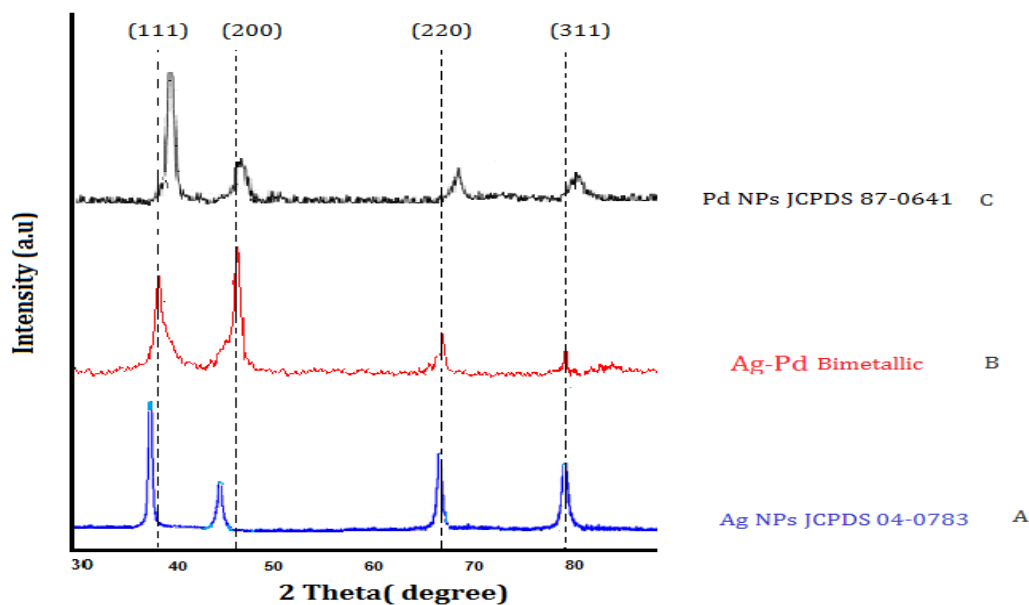
Figure 3.1:   XRD of Ag NPs (A), Pd NPs (B), Ag-Pd Bimetallic nanoparticles (C)

XRD of green synthesized Ag-Pd bimetallic nanoparticles is shown in Figure 3.1. The XRD of bimetallic was compared with monometallic Ag and monometallic Pd nanoparticles. Silver monometallic nanoparticles diffraction peaks were appeared at 38.048°, 44.5° and 65.27°, 77.45° correspond to (111), (200) and (220) and (311) diffraction planes according to JCPDS file 04-0783 of silver [114]. XRD peaks of monometallic palladium nanoparticles were appeared at 40.2°, 46.4° and 68.05° according to JCPDS file number 87-0641[115]. XRD diffraction patterns of Ag-Pd bimetallic nanoparticles were obtained at 39.05°, 46.3° and 66.3° and 77.8° correspond to (111), (200) and (220) and (311) respectively, that are appeared at 2θ range of monometallic silver nanoparticles and no individual Pd and Ag peaks were present in the spectrum and with the addition of palladium into Ag nanoparticles, the diffraction peaks shifted to larger angle as compare to monometallic silver nanoparticles, indicating the bimetallic structure of Ag-Pd nanoparticles. XRD data analysis has confirmed Ag-Pd nanoparticles have face-centered cubic structure**.**

Table 3.1: Average Crystallite size of Ag-Pd bimetallic nanoparticles

Average crystllite size of Ag—Pd nanoparticles (nm)		
hkl	2θ	Crystallite size
(111)	39.0	4.5 nm
(200)	46.3	9.3 nm
(220)	66.3	9.9 nm
Average crystallit size		7.9 nm

Crystallite size was calculated by Debye Scherrer equation:

$$D=K\lambda/\beta Cos\Theta$$

Where λ= 1.54E-10m for Cu-Kά radiations, K is shape factor whose value is equal to 0.8-0.9. ß is Full Width at Half Maxima .Its value was equal to 0.85 for (200) plane of Ag-Pd bimetallic nanoparticles. It is converted to radian by following:

Converted ß into radian   0.85 x π/ 180

0.85 x 3.14/180

ß=0.01487 rad.

Particle size for peak 46.29 (200) is calculated as:

2Θ= 46.3 from peak position

Θ = 46.3 /2= 23.15 put in Debye Scherrer equation

D=(0.9x1.54E-10)/0.01487Cos(23.15)

D=9.3 nm

Particle size for diffraction planes (200) was 9.3 nm. Similarly the crystallite size for (111) and (220) diffraction planes was calculated as 4.5nm and 9.9nm respectively. The average crystallite size was calculated as 7.9 nm as given in Table 3.1.

Lattice constant for all the diffraction planes of bimetallic nanoparticles was calculated .For diffraction plane (111) lattice constant was calculated as follow:

$$d= \lambda/2Sin\theta$$

2θ=39.055

$$d_{hkl}=2.3036\text{Å}$$
$$d_{hkl}=a/(h^2+k^2+l^2)^{1/2}$$
$$\textbf{a=3.9899 Å}$$

So for diffraction plane Å / (111), lattice constant is 3.9899 Å.

XRD peaks of bimetallic nanoparticles were broad band and they were in the overlap region of monometallic Ag and Pd nanoparticles. While XRD peaks of monometallic were fairly sharp that confirmed bimetallic nanoparticles formation.

3.1.3 FTIR Analysis of Ag-Pd Bimetallic Nanoparticles

In order to confirm polyphenolic biomolecules of *Camellia sinensis* extract, involved in capping and reduction of bimetallic NPs and their interaction with surface of Ag-Pd bimetallic nanoparticles, FTIR analysis was performed by using Alpha (BRUKER) Spectrophotometer in the range of 4000 to 500 cm^{-1}. The FTIR spectrum of Ag-Pd bimetallic nanoparticles was obtained by forming a thin KBr pellet .
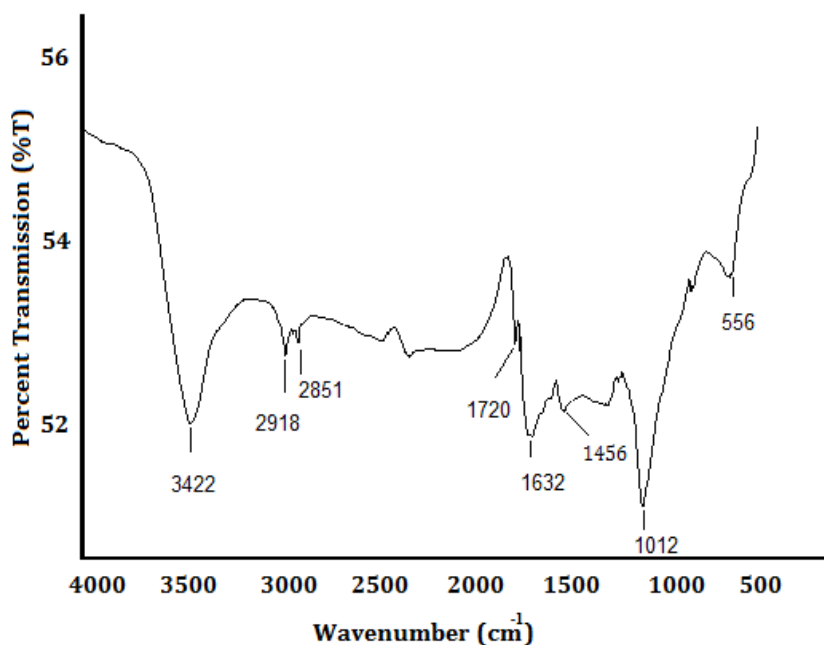
Figure 3.2: FTIR of Ag-Pd bimetallic nanoparticles

FTIR spectrum of bimetallic nanoparticles showed several bands in different regions, indicating several biological species are responsible for reduction as shown in Figure 3.2. The IR band that was observed in the region of 3422 cm^{-1} is due to stretching vibration of O-H group in polyphenols [116]. The bands at 2918 cm^{-1} and 2851 cm^{-1} are due to C-H stretch in alkanes and 0-H stretch in carboxylic acid respectively. The band at 1720 cm^{-1} and 1632 cm^{-1} are assigned to C=O stretch in esters and C=O stretch in polyphenols present in green tea extract respectively [116]. Bands appeared at 1456 cm^{-1} and 1012 cm^{-1} are due to stretching vibration of amine –NH stretch in protein and C-O-C stretch in polysaccharides, present in green tea extract respectively [117,118]. A broad band appeared at 556 cm^{-1} in a metal complex region is due to Ag-Pd bimetallic nanoparticles. From the above observation it can be concluded that high percentage of polyphenolic groups in green tea are responsible for reduction process and carbohydrates, amino acids and proteins are responsible for stabilization of nanoparticles.

3.1.4 Energy Dispersive X-ray Spectroscopy

Formation of bimetallic NPs was further confirmed by EDX analysis. Elemental composition of Ag-Pd nanoparticles was determined from EDX data as shown in Figure 3.3.
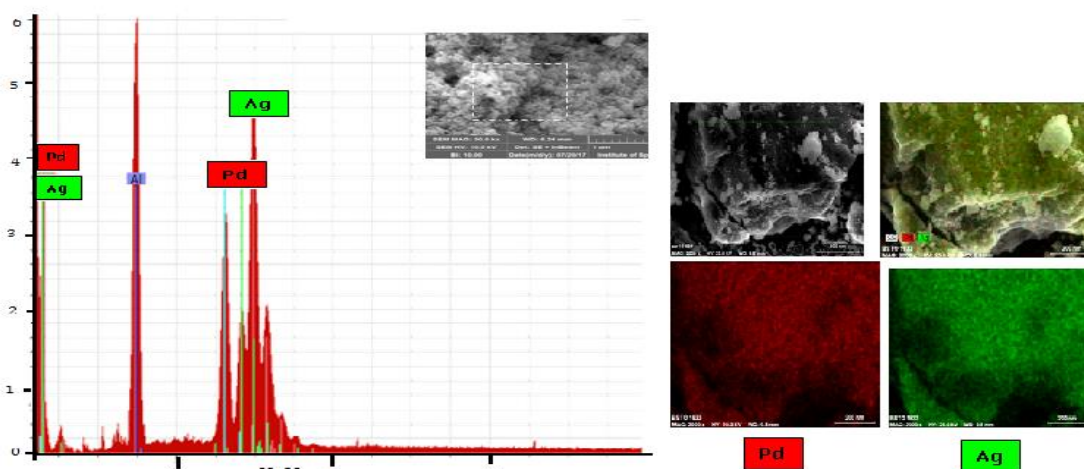
Figure 3.3: EDX spectrum and elemental mapping of Ag-Pd Bimetallic   Nanoparticles

EDX spectrum of Ag-Pd is shown in Figure 3.4. Presence of both Ag and Pd nanoparticles is evident from the spectrum. Composition of Ag-Pd nanoparticles was calculated as 73.13 atomic % for silver and 26.87 atomic % for palladium nanoparticles. Along with Ag and Pd peaks, Al peak was also appeared that is related to grid. Presence of both Ag and Pd nanoparticles was further confirmed by elemental mapping. Ag nanoparticles are represented by green color while palladium nanoparticles with red.

3.2   Synthesis and Characterization of Polypyrrole

Polypyrrole was synthesized and its synthesis was confirmed by X-ray diffractometry and Fourier Transform Infrared Spectroscopy.

3.2.1 Synthesis of Polypyrrole

Polypyrrole is widely acceptable polymer due to its ease of synthesis. Polypyrrole was synthesized by chemical polymerization of pyrrole monomer using $FeCl_3$ as an oxidant in the presence of chloroform as a solvent. Polypyrrole was obtained in the form of black powder as a result of free radical polymerization of pyrrole monomer. It was further characterized by XRD and FTIR analysis.

3.2.2 X-ray Diffraction Analysis of Polypyrrole

The crystalline structure and synthesis of polypyrrole was confirmed by X-ray analysis by using Rigaku X-ray diffractrometer, with CuK_α radiation source, having wavelength (λ) equal to 0.154 nm, equipped with graphite monochromator in a 2θ range of 5°-90° with 0.05 step size at a time count of 1 second. All the diffraction analysis was done at room temperature under constant conditions.
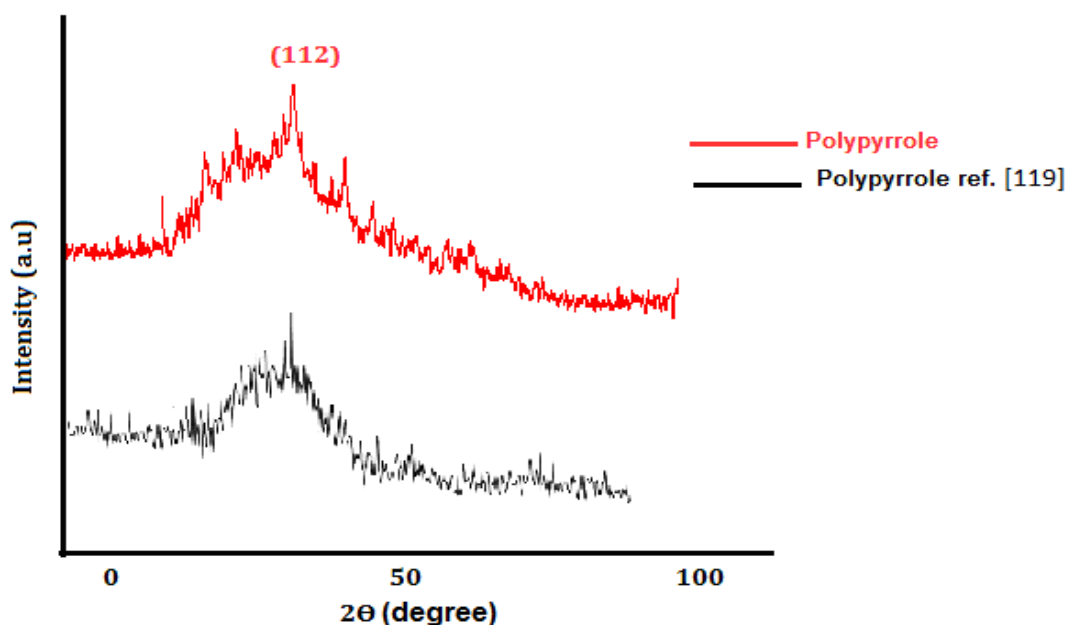
Figure 3.4: XRD pattern of PPy (Red) matched well with PPy reference (Black)

XRD pattern of polypyrrole matched well with reference [119] as shown in Figure 3.4. Polypyrrole exhibited a characteristic peak at $2\theta = 24.5$ °, which can be assigned to repeating units of pyrrole ring. The broad peak reveals the amorphous nature of polypyrrole rather than crystalline, which is mostly due to scattering from polypyrrole chains at the interplanar spacing [118].

Chain separation for the high intensity peak can be calculated by using formula [119]:

$$S = 5\lambda/8Sin\theta$$

Where λ is wavelength of X-ray and θ is the angle of high intensity peak and S is chain separation. The chain separation was calculated as 4.53 Å.

3.2.3 FTIR Analysis of Polypyrrole

FTIR analysis was performed by using Alpha (BRUKER) Spectrophotometer in the range of 4000 to 500 cm^{-1}. FTIR spectrum of polypyrrole showed several bands in different regions as shown in Figure 3.5.
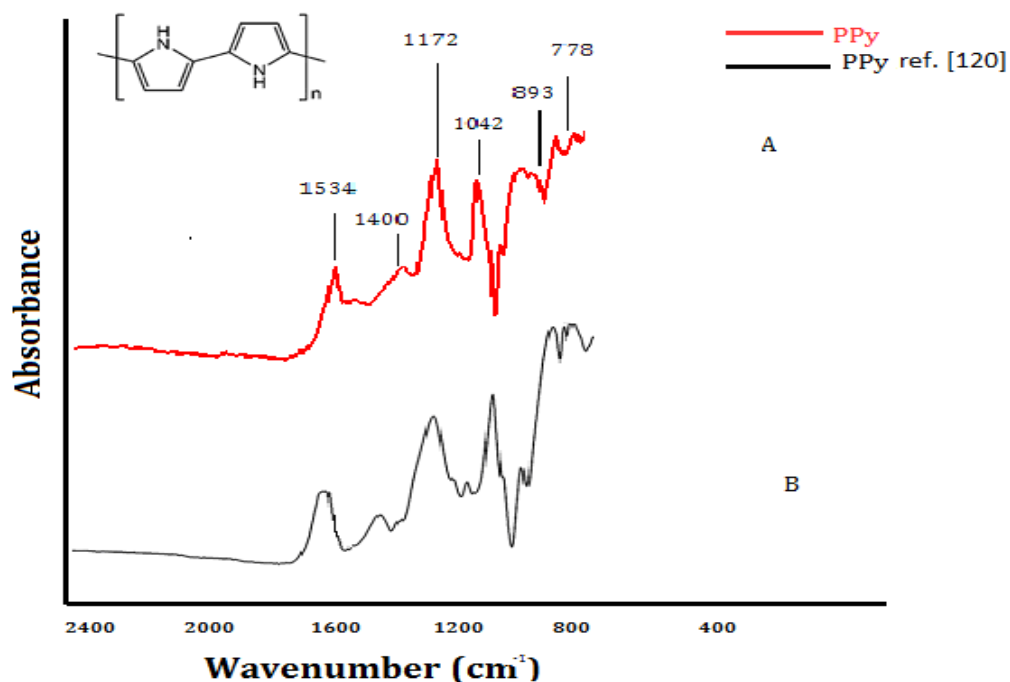
Figure 3.5: FTIR spectrum of PPy (A) matched well with PPy reference (B)

The band appeared at 1534 cm^{-1} and 1400 cm^{-1} are correspond to C=C and C=N vibration of pyrrole ring [120] . The band at 1172 cm^{-1} is assigned to C-N stretch bending. Band around 1042 cm^{-1} is correspond to out-of plane vibration of =C-H while 893 cm^{-1} is assigned to =C-H in-plane vibration. Band attributed to C-H wagging vibration is appeared at 778 cm^{-1}. FTIR spectrum of polypyrrole matched well with that of the reference [120]. FTIR results have confirmed the synthesis of polypyrrole.

3.3 Synthesis and Characterization of PPy/SIS Blends

3.3.1 Synthesis of PPy/SIS Blends

Blends of polypyrrole with SIS copolymer were synthesized using solution blending technique. Polypyrrole was loaded into pure SIS copolymer in different weight percent, ranging from 0 -20 wt. % by using chloroform as a solvent. The mixture was stirred for 24 hours without heating. In order to cast a film mixture was poured into Teflon Petri dish and placed overnight to evaporate the solvent. After that films were dried in a

vacuum oven. Incorporation of polypyrrole into SIS copolymer was confirmed by FTIR analysis.

3.3.2   FTIR Analysis of PPy/SIS Blends

FTIR analysis was performed by using Alpha (BRUKER) spectrophotometer in the range of 4000 to 500 cm^{-1}.ATR technique provides useful surface information of a sample. The FTIR spectrum of PPy/SIS blend was clearly different from that of original SIS copolymer, especially in the region between 1092 to 877 cm^{-1} as shown in Figure 3.6. In case of pure SIS copolymer, bands appeared at 2962 cm^{-1} and 2921 cm^{-1} are assigned to C-H symmetrical and C-H asymmetrical stretching in aromatic ring respectively. The band at 2846 cm^{-1} was correspond to C-H stretching vibration in aliphatic chain of SIS copolymer. Bands appeared at 1645, 1597 and 1442 cm^{-1} are assigned to C=C stretching in aromatic ring, C=C stretching in alkenes and C-H bending in aliphatic chain of SIS copolymer respectively. C-H in-plane and C-H out-of plane stretching vibrations were observed at 1085 and 757 cm^{-1} respectively.
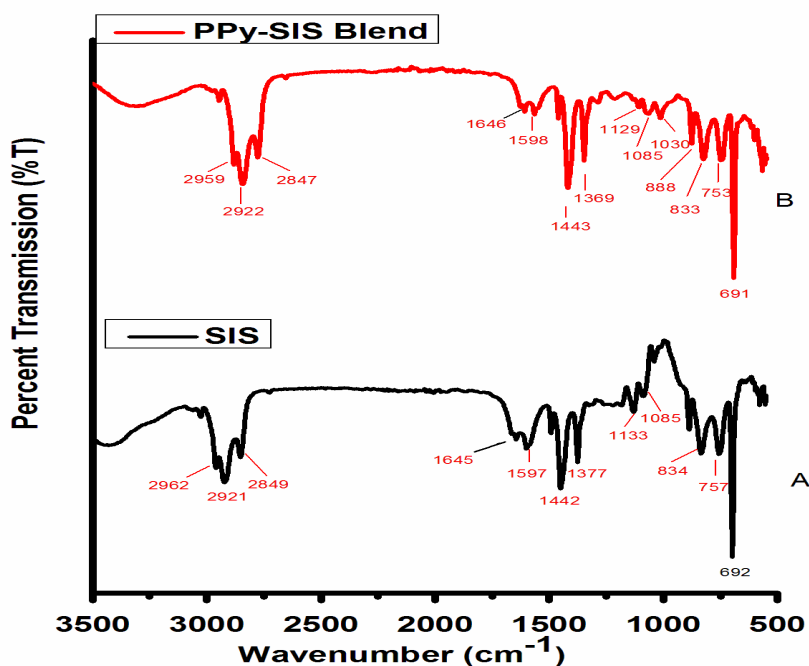
Figure 3.6: FTIR spectrum of pure SIS (A) and PPy/SIS blend (B)

Band at 834 cm^{-1} was assigned C=CH$_2$ stretching vibration in SIS copolymer as shown in Figure 3.8 (A). When polypyrrole was incorporated into SIS blend, the band positions shifted slightly with decrease in intensity as shown in Figure 3.6 (B). A new band appeared at 1030 cm^{-1} is correspond to N-H deformation of polypyrrole [45]. The difference is clearly observed in the region between 1092-877 cm^{-1}, when both spectrums were merged as shown in Figure 3.7. All the changes in bands position, band intensities and appearance of new bands have confirmed the physical blending of two polymers.
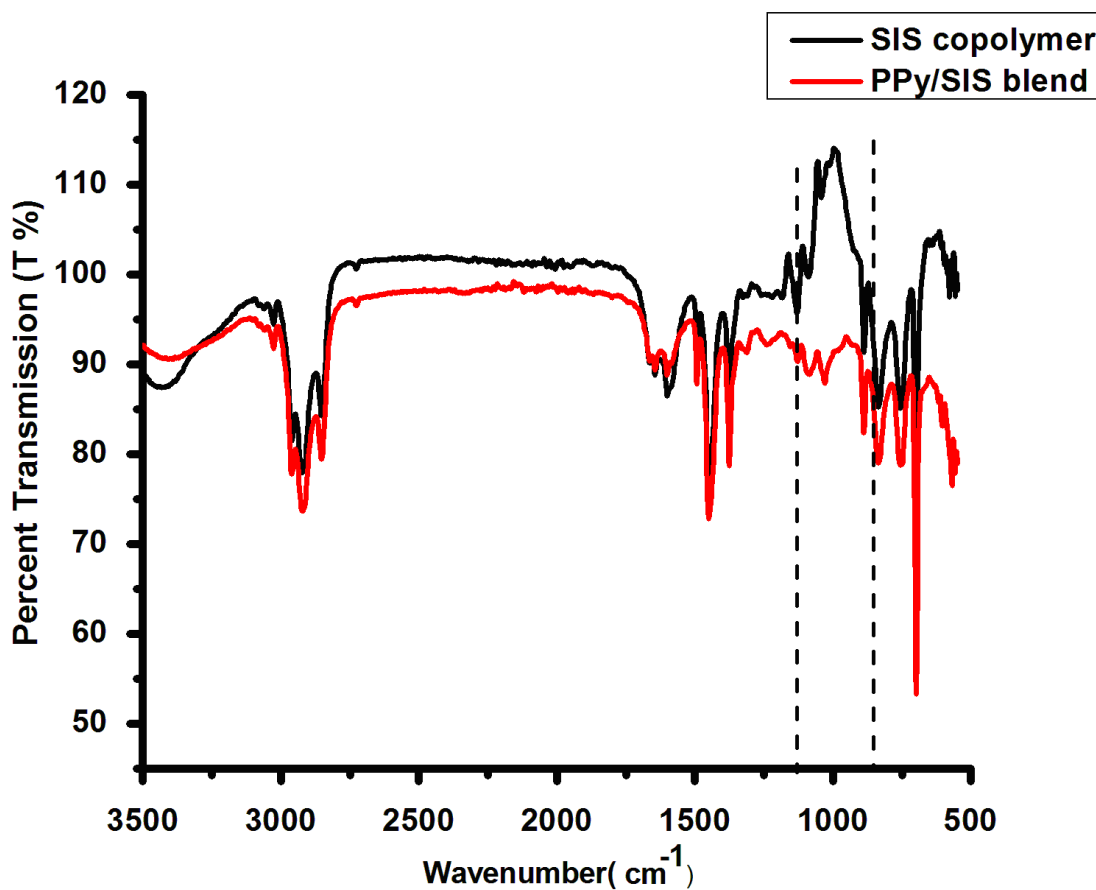
Figure 3.7: Merge FTIR spectrum of SIS copolymer (Black) and PPy/SIS blend (Red)

3.4 Synthesis and Characterization of Ag-Pd/PPy-SIS Nanocomposites

3.4.1 Synthesis of Ag-Pd/PPy-SIS Nanocomposites

Nanocomposites of Ag-Pd/ PPy-blend-SIS were prepared by adding bimetallic nanoparticles as reinforcement to the PPy-blend-SIS. In this case PPy-blend-SIS matrix phase properties are enhanced by bimetallic reinforcement. The composition of nanocomposites varied between 1-5 % by weight of Ag-Pd nanoparticles.

3.4.2 Mechanical Testing of Polypyrrole /SIS Blends and Ag-Pd/PPy-SIS Nanocomposites

To measure the change in mechanical properties of SIS copolymer with the addition of polypyrrol, tensile test was performed for each blend as well as for pure SIS copolymer. The test was done according to ASTEM D882 by using SHIMADZU Tensile Testing Machine available in SCME mechanical testing lab, NUST , at a test rate of 5 mm/min. ASTEM D882. The effect of loading different weight % of polypyrrole into thermoplastic SIS copolymer matrix was examined. The area under the stress-strain curve is related to energy required to break material. Effect of polypyrrole on Young's modulus, tensile stress and strain at break point was studied for each blend. Mechanical behavior of SIS blends with different wt. % of PPy is shown in Figure 3.8.
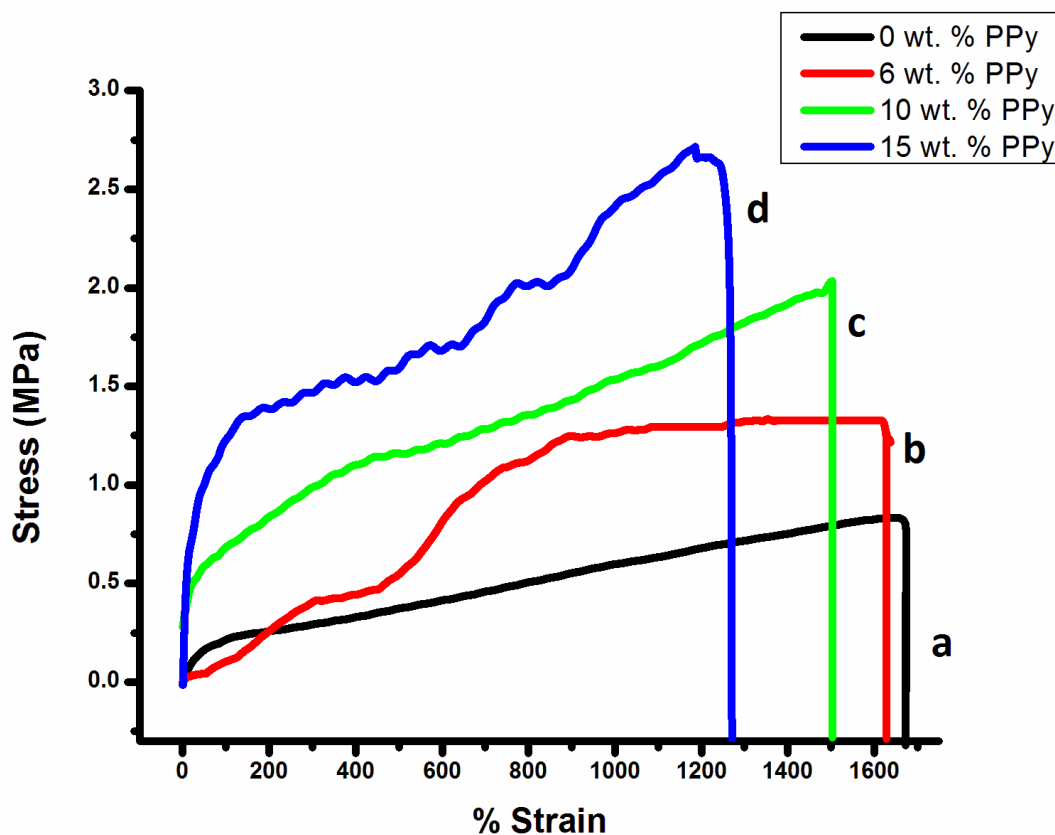
Figure 3.8: Stress vs. % Strain Curves for (a) 0 wt. % PPy/SIS, (b) 6 wt. % PPy/SIS , (c)10 wt. % PPy/SIS and (d) 15 wt. % PPy/SIS blends

Curve (a) shows the mechanical behavior of pure SIS copolymer. As pure SIS is very flexible at the test rate of 5mm/min and have large area under the stress-strain curve, indicating that great amount of energy is required to break the film. Young's modulus, tensile strength and % strain at break was calculated from curve and it was 0.13 MPa, 0.81 MPa and1676.93 % respectively.

Change in mechanical properties of SIS by the addition of PPy can be well understood from stress-strain curve of PPy/SIS blend illustrated in curve (b). As polypyrrole is very brittle in nature so addition of 6 wt. % polypyrrole into SIS caused a dramatic decrease in area under the curve, means less amount of energy was required to break the film. Stress of the film was gradually increased with the decreased in strain, by the addition of PPy. Young's modulus,

tensile strength and % strain at break point was calculated as 0.17 MPa, 1.33 MPa and 1620.31 %.This shows that the brittle nature of PPy has prevented the elongation of SIS by increasing stress.

Curve (c) shows the mechanical behavior of blend with 10 wt. % PPy. It was observed that with the further addition of 10 wt. % of PPy into the SIS copolymer, there was a dramatic increase in stress from 1.33 to 2.0 MPa, with decrease in percentage strain from 1620 to 1500 %. The area under the curve was further reduced, indicating gradually increase in strength of a film as shown in Figure 3.11. Young's modulus, tensile strength and percentage strain was calculated as 0.24 MPa, 2.0 MPa and 1500 % respectively. This shows that the increased ratio of polypyrrole has further prevented the elongation of SIS copolymer by increasing Young's modulus along with stress.

As the amount of PPy was increased up to 15 wt. % , the area under the stress -strain curve was further reduced and the stress of the film was increased up to 2.7 MPa with decrease in percentage strain up to 1222 % as shown in curve (d). This indicates that the strength of the blend is continuously increasing by loading different weight percent of PPy and less amount of energy was required to break the material. Young's modulus of the film was increased up to 0.5 MPa.

This gradually increase in Young's modulus and tensile stress with decrease in % strain, shows that the addition of PPy in SIS copolymer enhanced the strength and stiffness of blend as shown in Table 3.2. The reason is that the incorporation of PPy into pure SIS copolymer causes disruption of polymer matrix and because of weak PPy interaction, even a small amount of PPy causes gradually decrease in percentage strain at a break point of pure SIS copolymer by decreasing flexibility. When PPy amount was increased further up to 20 wt. % instead of uniform distribution, agglomeration was observed.

Table 3.2 Young's modulus, Tensile stress and % Strain at break point for 0 wt. % PPy/SIS, 6 wt. % PPy/SIS , 10 wt. % PPy/SIS and 15 wt. % PPy/SIS Blends

Ppy contents Wt. %	Young's Modulus MPa	Tensile Strength M Pa	% strain at break
0	0.13	0.81	1676.93
6	0.17	1.33	1620.31
10	0.24	2.0	1500.53
15	0.5	2.71	1222.4

According to above results 15 wt. % PPy blend with SIS exhibited good mechanical properties. In order to study the effect of nanoparticles on the mechanical properties of SIS/15 wt. % PPy blend, Ag -Pd bimetallic nanoparticles were added as a nanofiller within the range of 1-5 wt.% .Similar test was repeated and effect of nanoparticles on Young's modulus, % strain and stress was reported as shown in Figure 3.9.
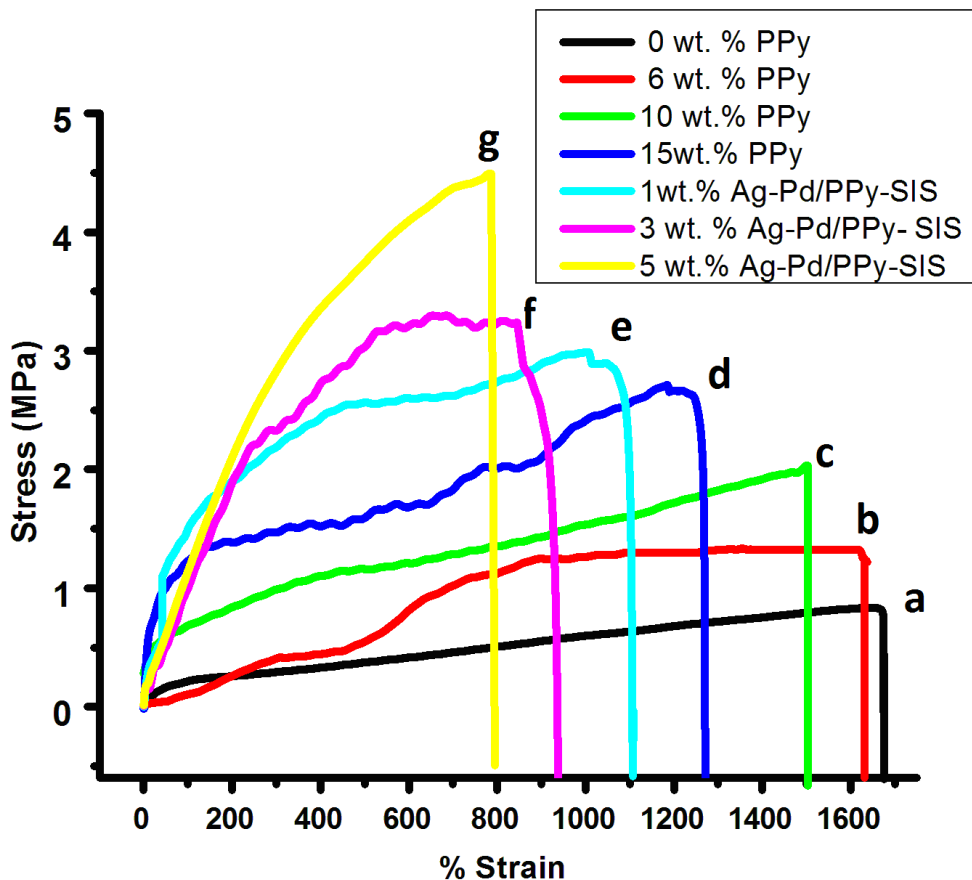
Figure 3.9: Stress vs. Strain curves for (a) 0 wt. % PPy/SIS, (b) 6 wt. % PPy/SIS , (c) 10 wt. % PPy/SIS, (d) 15 wt. % PPy/SIS, (e) 1 wt. % Ag-Pd/PPy-SIS, (f) 3 wt. % Ag-Pd/ PPy-SIS and (g) 5 wt. % Ag-Pd/ PPy-SIS nanocomposites

Curve (e) shows the effect of loading Ag-Pd nanoparticles on the mechanical behavior SIS-15 wt. % PPy. It was reported that with the further addition of 1 wt. % of nanoparticles into the SIS-PPy blend, there was a dramatic increase in stress from 2.71 to 2.9 MPa with decrease in percentage strain from 1222.4 % to 1099 %. The area under the curve was further reduced, which shows that the less amount of energy was required to break the film and the Young's modulus was increased up to 2.5 MPa indicating gradually increase in strength of a film. This shows that loading of nanoparticles have further prevented the elongation of SIS-PPy film by increasing Young's modulus along with stress.

Curve (f) shows the mechanical behavior of 3 wt. % Ag-Pd/PPy-SIS nanocomposite. It was reported that with the further addition of 10 wt. %of PPy into the SIS copolymer, there was a dramatic increase in stress from 1.33 to 2.0 MPa with decrease in percentage strain from 1620 to 1500 %. The area under the curve was further reduced, and less amount of energy was required to break the film indicating gradually increase in strength of a film as shown in Figure 3.15. Young's modulus, tensile strength and percentage strain was calculated as 0.24 MPa, 2.0 MPa and 1500 % respectively. This shows that the increased ratio of polypyrrole has further prevented the elongation of SIS copolymer by increasing Young's modulus along with stress. When 5 wt. % NPs were loaded the stress was increased up to 4.46 MPa from 2.71 MPa with the decrease in % strain 1222 to 786 %. It was observed that by increasing the amount of nanoparticles into SIS/ 15 wt. % PPy, the area under the curve was reduced further with the dramatic increase in tensile stress and decrease in percentage strain as shown in curve (g). This shows that Incorporation of nanoparticles into a blend have increased the stiffness and strength of nanocomposite while limiting the elongation of SIS , as nanoparticles are in nanometer range, that have a tremendous effect on the mechanical properties of a material as compare to that of composite. Nanocomposites show good results as compare to blends without nanofiller as shown in Figure 3.9.

Young's modulus, stress and % strain at fracture point is shown in Table 3.3 both for blends and nanocomposites and gradually increase in strength can be easily observed.

Table 3.3: Young's modulus ,Tensile strength and % strain at break point for 0 wt. % PPy/SIS, 6 wt. % PPy/SIS , 10 wt. % PPy/SIS, 15 wt. % PPy/SIS and 1 wt. %Ag-Pd/SIS-PPy,3wt.%Ag-Pd/SIS-PPy and 5wt.% Ag-Pd/SIS-PPY nanocomposites

Ppy contents Wt. %	Young's Modulus MPa	Tensile Strength M Pa	% strain at break
0	0.13	0.81	1676.93
6	0.17	1.33	1620.31
10	0.24	2.0	1500.53
15	0.5	2.71	1222.4
1 wt. %NPs	2.5	2.9	1099
3 wt. % Nps	2.7	3.26	995
5 wt. % NPs	3.1	4.45	786

3.4.3   Electrical Conductivity Measurements

Effect of polypyrrole incorporation on electrical conductivity of thermoplastic SIS matrix was studied by two point method. Electrical resistance of two point was measured by Agilent 4339 High Resistance Meter at 5 volts. All the data was obtained at room temperature. The amount of polypyrrole in SIS blend was varied in the range of 6-20 weight percent.
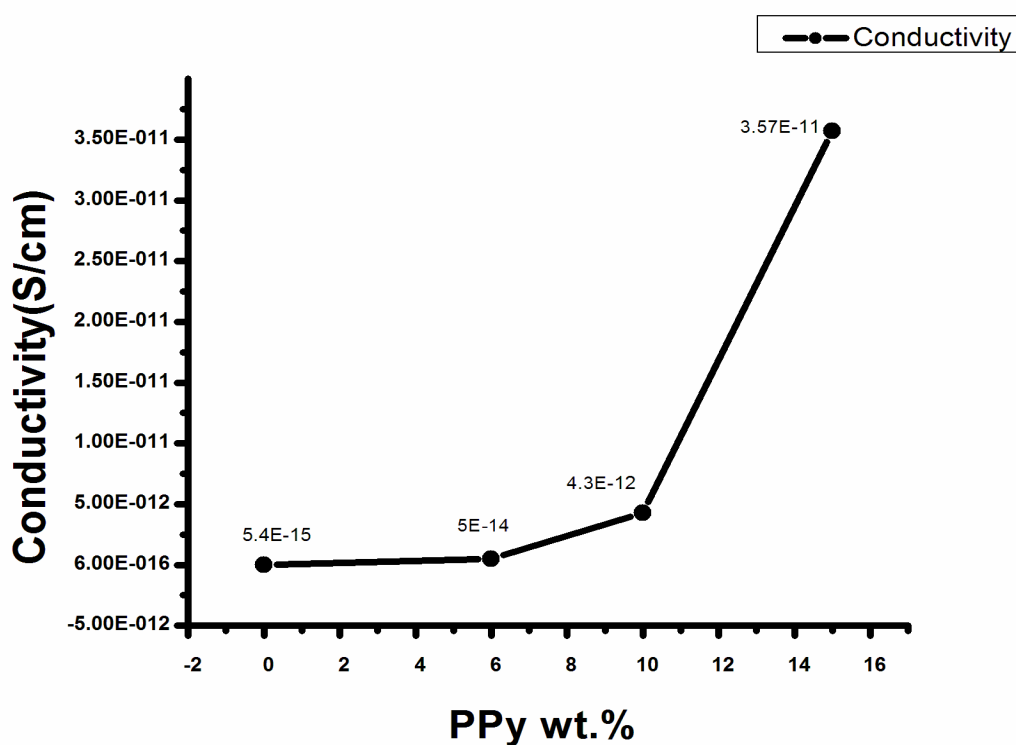
Figure 3.10: Conductivity Curve of 0 wt. %PPy/SIS blend, 6wt.% PPy/SIS, 10 wt.% PPy/SIS and 15 wt. % PPy/SIS without nanoparticles

Figure 3.10 shows electrical conductivity of PPy/SIS blends with different weight % of polypyrrole without the addition of nanoparticles .The electrical conductivity of pure SIS was measured as 5.4E-15 S/cm. When 6 wt. % polypyrrole was added the conductivity of blend is increased up to 5E-14 S/cm. Increase in conductivity of pure SIS is clearly observed .When 10 weight percent polypyrrole was loaded into SIS copolymer the

conductivity was increased further up to 4.3 E-12. With the addition of 15 weight % polypyrrole into SIS copolymer the electrical conductivity was increased up to 3.7 E-11 S/cm .The above results of conductivity show that blend with 15 wt.% PPy exhibited best results.

To study the effect of nanoparticles on the electrical properties of SIS/15 wt. % PPy blend, Ag -Pd bimetallic nanoparticles were added as nanofiller within the range of 1-5 wt. % and similar test was repeated.
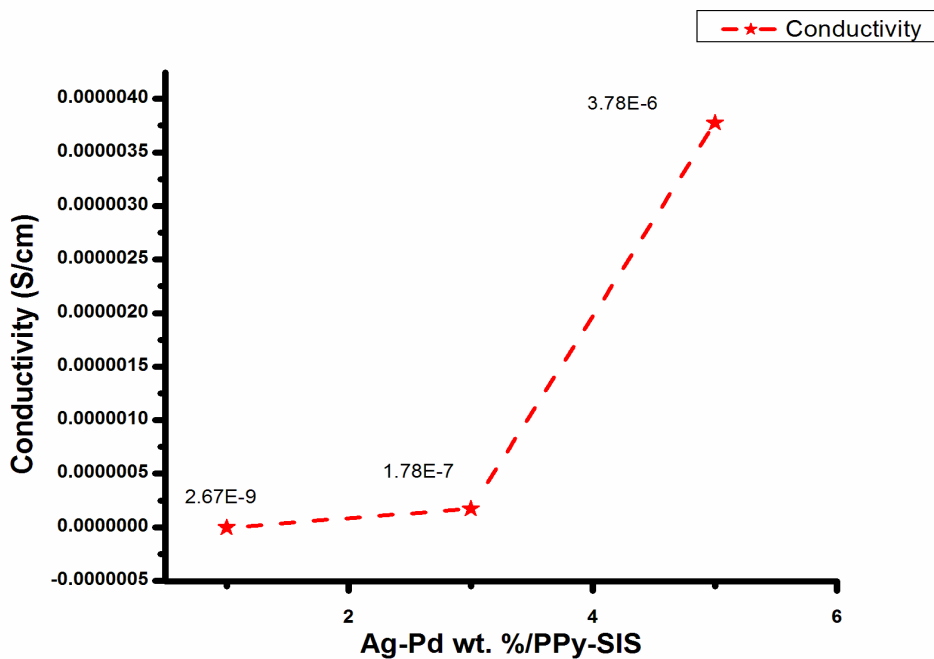
Figure 3.11: Conductivity Curve for 1 wt. % Ag-Pd/PPy-SIS, 3 wt. % Ag-Pd/PPy-SIS and 5 wt. % Ag-Pd/PPy-SIS

Figure 3.11 shows the electrical measurements of Ag-Pd/ 15 wt. %PPy-SIS nanocomposite. When 1 wt. % Ag-Pd nanoparticles were added in to 15 wt% PPy/SIS blend, the electrical conductivity was increased from 3.7 E-11 S/cm up to 2.67 E-9 S/cm. With the further addition of 3 wt. % and 5 wt. % nanoparticles the conductivity was calculated as 1.78E-7 S/cm and 3.78 E-6 S/cm respectively. A tremendous increase in conductivity is observed with 5 weight percent nanoparticles.

Table 3.4: Electrical conductivity of PPy/SIS blend (A) Electrical conductivity of Ag-Pd/15 wt. % PPy-SIS

A: Wt.% PPy/SIS Blend	Conductivity (S/cm)
0 wt. % PPy	5.4E-15
6 wt.% PPy	5E -14
10 wt. % PPy	4.3 E-12
15wt % PPy	3.7 E-11

B: wt.% Ag–Pd/15 wt % PPy	Conductivity (S/cm)
1 wt.% Ag–Pd	2.67 E-9
3 wt.% Ag–Pd	1.78E-7
5 wt.% Ag–Pd	3.78 E-6

The increase in conductivity with the addition of nanoparticles was observed and it is reported that Ag-Pd nanoparticles exhibited high electrical conductivity among different metals and they could act as a conductive junction between PPy chains that resulted in a high electrical conduction of PPy/SIS composite [121]. It is purposed that hopping process is responsible for high conductivity and wide range of localized states are created in a sample by the addition of Ag-Pd nanoparticles or high level of polaron and bipolarons are generated that caused characteristic distortion in a polymer backbone which playing a leading role in conductivity. By increasing Ag-Pd nanoparticles up to 5 wt.% , level of polaron and bipolarons may have increased and large number of localized states may be created that is the main reason for high conductivity [121].

3.5   Conclusion and Outlook

In this research work, Ag-Pd bimetallic nanoparticles were prepared by novel, cost effective and ecofriendly approach, using camellia sinensis extract. The XRD analysis has confirmed face centered cubic structure of nanoparticles with average crystallite size of 7.9 nm. The FTIR analysis has confirmed the presence of different functional groups on the surface of nanoparticles. Atomic composition of nanoparticles was calculated as 73.13 atomic % for silver and 26.87 atomic % for palladium by EDX analysis and it has confirmed presence of both Ag and Pd nanoparticles in a sample. Polypyrrole was synthesized by chemical polymerization of pyrrole monomer and its formation was confirmed by XRD and FTIR analysis. XRD analysis showed amorphous nature of polypyrrole with diffraction at $2\Theta=24.5°$. In FTIR spectrum characteristic bands due to stretching vibration of pyrrole were observed at 1534 cm^{-1} and 1400 cm^{-1} that confirmed the synthesis of polypyrrole. In the present research work polypyrrole/poly (styrene-isoprene-styrene) blends were formed for the first time to enhance processability of infusible polypyrrole. FTIR analysis has confirmed the incorporation of polypyrrole in to SIS copolymer. The tensile test and electrical conductivity results have shown that addition of polypyrrole has increased Young's modulus, tensile strength and conductivity of pure insulator SIS copolymer. The best tensile strength and conductivity results were reported with 15 wt.% PPy/SIS blends i.e. tensile strength was increased up to 2.71 MPa with increase in conductivity from 5.4 E-15 to 3.7 E-11 S/cm. Further enhanced electrical and mechanical properties were reported with the addition of Ag-Pd nanoparticles as a nanofiller i.e. mechanical strength was enhanced up to 4.5 MPa with the increased in conductivity up to 3.8 E-6 S/cm for 5 wt.% Ag-Pd/PPy-SIS nanocomposite.

Thermal stability of Ag-Pd/PPy-SIS nanocomposites has not been studied yet in this research work. In future thermal behavior of these nanocomposites will be study. As polypyrrole has wide range of applications in electronic devices and electronic industry is increasing day by day. Due to increasing number of electronic equipments there is a tremendous increase in microwave radiation associated with these equipment. These

Conclusion

microwaves interfere with other electronic devices near to them and may disturb their normal functioning. This type of interference is known as Electromagnetic Interference (EMI) and different shieldings are used to protect electronic devices from EMI. In recent years polymers have attracted researchers as an EMI shielding material and for such purpose the polymer should by conductor and have good mechanical strength. Polypyrrole/SIS blends with Ag-Pd nanofiller are a good candidate for EMI shielding and further magnetic behavior of blends can be increased using iron nanoparticles as filler. In future, this research may be focused on study of EMI shielding behavior of Ag-Pd/PPy-SIS nanocomposites.

Bibliography

1. V. R. Gowariker, N. Viswanathan and J. Sreedhar, *Polymer science*. New Age International, 1986.

2. R. J. Young and P. A. Lovell, *Introduction to polymers*. CRC press, 2011

3. E. Charles, and J. Carraher. *Polymer Chemistry*, Edited by J. J. LAGOWSKI, **Sixth Edition,** 2012.

4. K. Akagi, G. Piao, S. Kaneko, K. Sakamaki, H. Shirakawa and M. Kyotani. Helical polyacetylene synthesized with a chiral nematic reaction field. *Science*, **282** (5394):1683-1686, 1998

5. H. R. Kricheldorf, O. Nuyken, G. Swift. *Handbook of Polymer Synthesis,* 2005

6. A. Patil, A. Heeger and F. Wudl. Optical properties of conducting polymers. *Chemical Reviews* , **Vol.88 (**1):183-200, 1988.

7. H. Letheby. XXIX.—on the production of a blue substance by the electrolysis of sulphate of aniline*, J.Chem. Soc*.**, vol. 15**: 161-163, 1862.

8. J. W. P. Lin and L. P. Dudek. Synthesis and properties of poly (2, 5-thienylene), *Journal of Polymer Science Part A: Polymer Chemistry***, 18** (9): 2869-2873, 1980

9. A. J. Heeger. Semiconducting and metallic polymers: the fourth generation of polymeric materials (Nobel lecture), *Angewandte Chemie International Edition*,**40** (14): 2591-2611, 2001.

10. J. Burroughes, D. Bradley, A. Brown, R. Marks, K. Mackay, R. Friend, P. Burns and A. Holmes. Light-emitting diodes based on conjugated polymers, *nature*, **347** (6293): 539-541, 1990.

11. R. Kumar, S. Singh and B. Yadav .Conducting Polymers: Synthesis, Properties and Applications, *International Advanced Research Journal in Science, Engineering and Technology,***V ol. 2** (11): 110-124, 2015.

12. H. Shirakawa, E. J. Louis, A. G. MacDiarmid, C. K. Chiang and A. J. Heeger. Synthesis of electrically conducting organic polymers: halogen derivatives of polyacetylene,(CH) x, *Journal of the Chemical Society, Chemical Communications*, (16):578-580, 1977.

Bibliography

13. M. S. Freund and B. A. Deore, *Self-doped conducting polymers*. John Wiley & Sons, 2007.

14. W. Feast, J. Tsibouklis, K. Pouwer, L. Groenendaal and E. Meijer. Synthesis, processing and material properties of conjugated polymers, *Polymer,* **37** (22): 5017-5047, 1996.

15. Z. Li. *Synthesis and characterization of conducting polymer nanostructures and their application in sensors*. (Missouri University of Science and Technology, 2010).

16. J. L. Bredas and G. B. Street. Polarons, bipolarons, and solitons in conducting polymers *Acc. Chem. Res.,* **18**: 309, 1985

17. L. Dai. *Intelligent Macromolecules for Smart Devices: From Materials Synthesis to Device Applications Engineering Materials and Processes*, Springer Science & Business Media: 44-46, 2006.

18. Sevil, Baytekin, and Küçükyavuz Zuhal. Synthesis and characterization of polypyrrole nanoparticles and their nanocomposites with poly (propylene), *Macromolecular symposia.* Vol. 295(1): 20-21, 2010.

19. Y. Li. *Organic Optoelectronic Materials.* Technology & Engineering , 2015

20. M. F. M. Juan, V. C. Paya. *ELECTROCHEMISTRY–Conducting Polymers*, EOLSS Publications, 2009.

21. L.-X. Wang, X.-G. Li and Y.-L. Yang. Preparation, properties and applications of polypyrroles, *Reactive and Functional Polymers,* 47(2): 125-139, 2001.

22. R. McNeill, R. S., J.H. Wardlaw and D.S. Weiss. Electronic Conduction in Polymers: The Chemical Structure of Polypyrrole, *Aust. J. Chem*., **vol. 16**: 1056-1075,1963.

23. Conducting Polymershttp://homepage.ntlworld.comcolin.prattcpoly.pdf,last accessed on 13th May, 2009.

24. R. Ansari. Polypyrrole Conducting Electroactive Polymers: Synthesis and Stability Studies, *E-Journal of Chemistry* ,**Vol. 3**(4): 186-201. 2006.

25. S. Rapi, V. Bocchi and G. P. Gardini. Conducting polypyrrole by chemical synthesis in water, *Synth. Met.,* **vol**.24: 217,1988.

26. L. F. Warren and D. P. Anderson. Polypyrrole Films from Aqueous Electrolytes: The Effect of Anions upon Order*, Electrochemical Society,* **134**(1): 101-105, 1987.

Bibliography

27. G. Wallance, G. Spinks, L. Kane-Maguire and P. Teasdale. Conductive Electroactive Polymers, *Intelligent Materials Systems,2nd edition,CRC Press LCC, USA*: 51, 2003.

28. S. Goel, A. Gupta, K. Singh, R. Mehrotra, H. Kandpal, S. Samanta, S. Gayen, B. Ghosh, P. Panda and K. Srikanth. Structural and optical studies of polypyrrole nanostuctures, *International Journal of Applied Chemistry*, **Vol.2,(3):** 157-168, 2006.

29. X. Zhang and K. M. Sanjeev. Narrow pore-diameter polypyrrole nanotubes. *Journal of American Chemical Society*,**Vol.41**: 14156-14157.2005.

30. H. Wang, T. Lin, A. Kaynak. Polypyrrole nanoparticles and dye absorption propertie*, Synthetic Metals*, **Vol.151**: 136-140, 2005.

31. Y. Liu, Y. Chu and L. Yang. Adjusting the inner-structure of polypyrrole nanoparticles through microemulsion polymerization, *Materials Chemistry and Physics,* **Vol. 98**: 304-308,2006.

32. M. Amaike and H. Yamamoto. Preparation of polypyrrole by emulsion polymerization using hydroxypropyl cellulose. *Polymer journal* ,**38** (7): 703-709, 2006

33. M. Karim, C. Lee, and M. Lee. Synthesis of conducting polypyrole by radiolysis polymerization method*, Polymers for Advanced Technologies* **Vol.18**: 916-920, 2007.

34. T. H. Chao and J. March.Part A: Polymer chemistry , *J. Polymer Science*, **26**: 743-753,1988.

35. *Bocchi* and G. P. Gardini. *Chem. Soc.,Chem. commun.*,:148-156,1986.

36. Y. Xia, P. Yang, Y. Sun, Y. Wu, B. Mayers, B. Gates, Y. Yin, F. Kim and H. Yan. *Adv. Mater,***15** : 353, 2003

37. Y. Wei , X. Tag, and Y. Sun. *Polym. Sci., Polym. Chem. Ed***., Vol. 27**: 2385, 1989.

38. R. Kumar, S. Singh and B. Yadav.Conducting Polymers: Synthesis, Properties and Applications, *International Advanced Research Journal in Science, Engineering and Technology,***V ol. 2** (11): 3-4, 2015.

39. R. G. Kadhim, S. N. Sanaa, and S. H. Ahmed. Electrical and Mechanical properties Of (PVA-CMC-PEG) Blends, *Advances in Natural and Applied Sciences*, **9**(16): 12-18, 2015.

40. L. A. Utracki, and A. Charles. *Polymer Blends Handbook*, Dordrecht, The Netherlands: Kluwer Academic Publishers,2002.

41. E. Badum. *Ozone Resistant Cable Construction*, U.S. Patent: 2,297,194, 1942.

42. M. Khan, G. H. Albalawi, M. R. Shaik, M. Khan, S. F. Adil, M. Kuniyil, H. Z. Alkhathlan, A. Al-Warthan and M. R. H. Siddiqui *Polymer Blends. Handbook of Polymer Synthesis, Characterization, and Processing* :505-517. 2013

43. John Wiley & Sons. *Processing and Finishing of Polymeric Materials*, Technology & Engineering, Vol. **2:** 1488 , 2012.

44. V. S. Sangawar, and A. M. NEERAJA. Study of Electrical, Thermal and Optical Behavior of Polypyrrole Filled PVC:PMMA Thin Film Thermoelectric. *Chem Sci Trans* **, Vol.1**(2): 447-455, 2012.

45. V. Mano, *et al.*Thermal, mechanical and electrochemical behaviour of poly(viny/chloride)polypyrrole blends (PVC/PPy). *Polymer Wol.,* **Vol. 37** (23): 5165-5170,1996.

46. H. Wang, T. Lin and A. Kaynak Conducting Polymer Blends: Polypyrrole and Poly(viny1 methyl ketone) , *Macromolecules,* **Vol.25** : 6179-6184, 1992.

47. B. Sevil and K. Zuhal. Synthesis and characterization of polypyrrole nanoparticles and their nanocomposites with poly (propylene), *Macromolecular symposia,* Vol. 295(1): 22-24, 2010

48. S. Radhakrishnan and D. R. Saini. Structure and Electrical Properties of Polypyrrole-Thermoplastic Elastomer Blends*, Polymer International*, **Vol.34**: 111-117, 1994.

49. H. L. Wang, L. Toppare and J. E. Fernandez Conducting Polymer Blends: Polythiophene and Polypyrrole Blends with Polystyrene and Poly(bispheno1 A carbonate), *Macromolecules,* **Vol. 23:** 4, I990.

50. S. H. Hosseini, and A. A. Entezami. Conducting Polymer Blends of Polypyrrole with Polyvinyl Acetate, Polystyrene, and Polyvinyl Chloride Based Toxic Gas Sensors, *Journal of applied polymer science*, **Vol.**90.1:49-6, 2003.

51. J. Carraher, E. Charles. *Carraher's Polymer Chemistry*, Ninth Edition, CRC Press **:** 242-370, 2016.

52. N. R. Legge. Thermoplastic elastomers—three decades of progress*, Rubber Chem. Technol, Vol.***62**: 529-547, 1989.

Bibliography

53. B. J. Dair, et al. Mechanical Properties and Deformation Behavior of the Double Gyroid Phase in Unoriented Thermoplastic Elastomers , *Macromolecules*, **Vol.32**: 8145-8152, 1999

54. S. Feng, and X. Shen. Electrospinning and Mechanical Properties of Polystyrene and Styrene- Isoprene-Styrene Block Copolymer Blend Nanofibers. *Journal of Macromolecular Science, Part B: Physics,* **Vol.49** (2): 345-354, 2010

55. H. Li, X. Zeng and W. Wu. Epoxidation of Styrene-Isoprene-Styrene Block Copolymer and Its Use for Hot-Melt Pressure Sensitive Adhesives, *Polymer-Plastics Technology and Engineering* **,Vol.47**(10), 2008.

56. http://www.sigmaaldrich.com/technical-service-home.html.

57. C. Ngô and M. Van de Voorde. Nanotechnology *in a Nutshell: From Simple to Complex Systems*, Springer Science & Business Media **:** 54, 2014.

58. R. Hirsch. *Seizing the light: A history of photography*, 2000.

59. N.Taniguchi. On the basic concept of 'nano-technology'. In Proc. Intl. Conf. Prod. Eng. Tokyo. *Part II, Japan Society of Precision Engineering,* 1974.

60. J. Schiller. *Nanotechnology Development:Using Research from the Internet,* Create Space publisher, 197, 2010.

61. G. Binnig, and H. Rohrer. SCANNING TUNNELING MICROSCOPY, *Surface Science*, Vol. **126:** 236-244, 1983.

62. S. Hasan. A Review on Nanoparticles: Their Synthesis and Types, *Res. J. Recent. Sci.*, **Vol. 4**: 1-3, 2015.

63. C. Ngô and M. Van de Voorde.. *Nanotechnology in a Nutshell: From Simple to Complex Systems,* Springer Science & Business Media**:** 19-20, 2014.

64. *J. H. Sinfelt*, *J. Catal*, Vol. **29**:308,1973.

65. S. Dubchak, A. Ogar, J. Mietelski and K. Turnau. Influence of silver and tianium nanoparticles on arbuscular mycorhiza colonization and acumulation of radiocaesium in Helianthus anus, *Span. J. Agric. Res.,* **8**(1): 103-108,2010.

66. S. Horikoshi, and N. Serpone. *Microwaves in Nanoparticle Synthesis: Fundamentals and Applications*, John Wiley & Sons **:** 8, 2013.

Bibliography

67. M. N. Nadagouda and R. S. Varma. Green and controlled synthesis of gold and platinum nanomaterials using vitamin B2: density-assisted self-assembly of nanospheres, wires and rods, *Green Chem*. **Vol. 8**: 516-518, 2006.

68. Y. Y. Loo, B. W. Chieng, M. Nishibuchi, and S. Radu. Synthesis of silver nanoparticles by using tea leaf extract from Camellia Sinensis, *International Journal of Nanomedicine*, **Vol. 7:** 4263-4267, 2012.

69. M. N Nadagouda, and R. S. Varma. Green synthesis of silver and palladium nanoparticles at room temperature using coffee and tea extract, *Green Chem.***, Vol.10**: 859-862, 2008.

70. G. Pant, N. Nayak, and R. G. Prasuna. Enhancement of antidandruff activity of shampoo by biosynthesized silver nanoparticles from Solanumtrilo batum plant leaf, *Appl Nanosci* : 431-439, 2012.

71. T. Wang , J. L. Z. Chen , M. Megharaj , and R. Naidu . Green synthesized iron nanoparticles by green tea and eucalyptus leaves extracts used for removal of nitrate in aqueous solution*, Journal of Cleaner Production.***Vol.83:** 413-419, 2014.

72. K. Farhadi, R. E. Sabzi, M. Forough, A. Pourhossein, R. Molaei, and R. Ebrahimi. The $Ag_{core}Pd_{shell}$ bimetallic nanoparticles: simple biological synthesis and characterization, *J IRAN CHEM SOC*, **Vol.**12 **:** 2015-2021, 2015.

73. R. K. Petla, S. V. M. Misra, A. K. Mohanty, N. Satyanarayana. Soybean (Glycine max) Leaf Extract Based Green Synthesis of Palladium Nanoparticles, *Journal of Biomaterials and Nanobiotechnology,* **Vol.3**: 14-19, 2012.

74. W. S Khan, N. N. Hamadneh, and W. A. Khan. *Polymer nanocomposites - synthesis techniques, classification and properties*, Edited by P. P. D. Sia, One Central Press(OCP): 6-7, 2017.

75. L. S. Schadler, *In Nanocomposite Science and Technology*, Ajayan, PM; Schadler, L. S; Braun, PV, Eds. :140, 2003.

76. R. Asmatulu, W. S. Khan, R. J. Reddy, and M. Ceylan. Synthesis and Analysis of Injection-Molded Nanocomposites of Recycled High-Density Polyethylene Incorporated with Graphene Nanoflakes*, Polymer Composites,* **vol. 36 (9)** : 1565-1573, 2015.

Bibliography

77. Zhou, Hongjian, and Jaebeom Lee. Nanoscale hydroxyapatite particles for bone tissue engineering, *Acta Biomater,* **Vol. 7**: 2769-2781, 2011.

78. R. V. Kurahatti, A. O. Surendranathan, S. A. Kori, N. Singh, A. V. R. Kumar, and S. Srivastava . Defence Applications of PolymerNanocomposites, *Defence Science Journal* **,Vol. 60** (5): 551-563 , 2010.

79. J. Parameswaranpillai, N. Hameed, T. Kurian, and Y.Yingfeng .*Nanocomposite Materials: Synthesis, Properties and Applications,* CRC Press, 2016.

80. *P. H.* C. Camargo, K. *G. Satyanarayana*, *F*. Wypych. Nanocomposites: synthesis, structure, properties and new application opportunities, *Material Research,* **vol.12(1)**: 1-39, 2009.

81. E. T. Thostenson, L. Chunyu and T. Chou. Nanocomposites in context, *Composites Science and Technology*, **vol.65**: 491-516, 2005.

82. J. Jordon, K. I. Jacob , R.Tannenbaum, M. A. Sharaf, I. Jasiuk. Experimental trends in polymer nanocomposites- a review, *Material Science and Engineering A.,* **vol. 393**: 1-11, 2005

83. T. Kurauchi, A. Okada, T. Nomura, T. Nishio, S. Saegusa, and R. Deguchi. *Nylon 6-clay hybrid-synthesis, properties and application to automotive timing belt cover.* No. 910584. SAE Technical Paper, 1991.

84. J. W. Gilman, T. Kashiwagi, and J. D. Lichtenhan . Nanocomposites: a revolutionary new flame retardant approach, *SAMPE Journal*, **Vol.33(4)**:40-46, 1997.

85. L. Rapoport, O. Nepomnyashchy, A. Verdyan, R. Popovitz-Biro, Y. Volovik, Baruth Ittah, and R. Tenne. Nanocomposites with Fullerene-like Solid Lubricant, *R. Polymer Adv. Engg. Mater,* **6(1-2)**: 44-48, 2004.

86. M. Tanahashi. Development of Fabrication Methods of Filler/Polymer Nanocomposites: With Focus on Simple Melt-Compounding-Based Approach without Surface Modification of Nanofillers, *Materials Chemistry and Physics*, **vol. 3(3)**: 1593-1619, 2010.

87. R. A Kalgaonkar. *Polymer nanocomposites based on amorphous copolyster and organo-inorganic nanofillers: a structure and property study*. *Polymer Science and Engineering Division National Chemical Laboratory (NCL)* .UNIVERSITY OF PUNE, 2007.

88. B. Sevil, K. Zuhal. Synthesis and characterization of polypyrrole nanoparticles and their nanocomposites with poly (propylene), *Macromolecular symposia.* Vol. 295(1), WILEY-VCH Verlag, 2010.

89. R. R. Jannapu. Preparation, Characterization and Properties of Injection Molded Graphene Nanocomposites, *Mechanical Engineering*, Wichita State University, Wichita, Kansas, USA. **Master's thesis,** 2010.

90. J. Srivastava, P. K. Khanna, P. V. More, and N. Singh. Chemically synthesized Ag/PPy-PVA polymer nanocomposite films as potential EMI shielding material in X-band, AdvancedMaterials L etters **, Vol.8(1):** 42-48, 2017.

91. P. Dallas, D. Niarchos, D. Vrbanic, N. Boukos, S. Pejovnik, C. Trapalis, and D. Petridis. Interfacial polymerization of pyrrole and in situ synthesis of polypyrrole/silver nanocomposites, *Polymer* **48**: 2007- 2013, 2007.

92. M. F. Ghadim, A. Imani, and G. Farzi. Synthesis of PPy–silver nanocomposites via in situ oxidative polymerization, *J Nanostruct Chem., Vol. 4* : 101, 2014.

93. R. Gupta, K. Jayachandran, J. S. Gamare, B. Rajeshwari, S. K. Gupta, and J. V. Kamat. Novel Electrochemical Synthesis of Polypyrrole/Ag Nanocomposite and Its Electrocatalytic Performance towards Hydrogen Peroxide Reduction , *Journal of Nanoparticles,* Vol. **2015:** 6, 2015.

94. V. T. Bhugul, and G. N. Choudhari. Synthesis and Studies on Nanocomposites of polypyrroleAl- doped zinc oxide Nanoparticles, *International Journal of Scientific and Research Publications***, Vol. 5(1),** 2015.

95. P. K. Khanna, S. B., V. Dhanwe, A. Kshirsagara and P. Morea. In situ SeO2 promoted synthesis of CdSe/PPy and Se/PPy nanocomposites and their utility in optical sensing for detection of Hg^{2+} ions, *RSC Advances.,*(113), 2015.

96. Y. S. Lin, , Y. J. Tsai, J. S. Tsay, and J. K. Lin. Factors affecting the levels of tea polyphenols and caffeine in tea leaves, *Journal of agricultural and food chemistry* , **51(7):** 1864-1873, 2003.

97. C. Cabrera, R. Artacho, and R. Giménez. Beneficial Effects of Green Tea-a Review. *Journal f the American College of Nutrition,* **25**(2): 79-99, 2006.

Bibliography

98. A. A. Bunaciu, E. G. UdriŞTioiu and H. Y. Aboul-Enein. X-ray Diffraction: Instrumentation and Applications, *Critical Reviews in Analytical Chemistry ,* **Vol.**45: 289-299, 2015

99. D. E. Robin. Implementation, Analytical Characterization and Application of a Novel Portable XRF/XRD Instrument. (2012).

100. A. A. Bunaciu, E. G. UdriŞTioiu and H. Y. Aboul-Enein. X-ray Diffraction: Instrumentation and Applications, *Critical Reviews in Analytical Chemistry ,* **Vol.**45: 289-299, 2015.

101. K. D. Harris, and M. Tremayne. Crystal structure determination from powder diffraction data, *Chemistry of materials*, Vol. 8(11) : 2554-2570, 1996.

102. G. Poralan Jr, J. Gambe, E. Alcantara and R. Vequizo . X-ray diffraction and infrared spectroscopy analyses on the crystallinity of engineered biological hydroxyapatite for medical application, *Materials Science and Engineering,* **Vol**.79, 2015.

103. S. *Swapp. Scanning Electron Microscopy (SEM)*, University of Wyoming: 1-4, 2013.

104. M. T. Postek, S. H Karen, H. J Arthur, and L. M. Kathlyn. *Scanning Electron Microscopy: A Student's Handbook, Ladd Research Ind.,* Inc. Williston, VT., 1980.

105. A. Kaech, Introduction to electron microscopy, *Center for Microscopy and Image Analysis*, University of Zurich**:** 16-17, 2013.

106. J. Goldstein. *Scanning electron microscopy and X-ray microanalysis*, Kluwer Adacemic/Plenum Pulbishers: 689 , 2003.

107. R. M. Silverstein, X. W. Francis, J. K. David and L. B. David. *Spectrometric Identification of Organic Compounds*, John wiley & sons, 2014.

108. I. S. Boziaris, ed. *Novel Food Preservation and Microbial Assessment Techniques* , CRC Press, 2014

109. S. F. Wang , Y. F. Hsu, Y. W. Hung, and Y. X. Liu. Effect of Ta_2O_5 and Nb2O5 Dopants on the Stable Dielectric Properties of $BaTiO_3$-(Bi0.5Na0.5)TiO_3-Based Materials , *Appl. Sci.,* **Vol. 5:** 1221-1234, 2015.

110. Y. Singh . Electrical resistivity measurements: a review, *International Journal of Modern Physics: Conference Series*, **Vol. 22:** 745-756, 2013.

Bibliography

111.   R. B. D. Dickey. Determination of Diffusion Characteristics Using Two- and Four-Point Probe Measurements California, Solecon Laboratories

112.   A. Nayar. Testing of Metals, Tata McGraw- Hill Education**:** 202 pages, 2005.

113.   Annual Book of ASTM Standards, Vol 08.01.

114.   M. Khan, G. H. Albalawi, M. R. Shaik, M. Khan, S. F. Adil, M. Kuniyil, H. Z. Alkhathlan, A. Al-Warthan and M. R. H. Siddiqui. Extensive Studies on X-ray Diffraction of Green Synthesized Silver Nanoparticles, *Advances in Nanoparticles*, **Vol. 4**: 1-10, 2015.

115.   M. Khan, G. H. Albalawi, M. R. Shaik, M. Khan, S. F. Adil, M. Kuniyil, H. Z. Alkhathlan, A. Al-Warthan and M. R. H. Siddiqui. Miswak mediated green synthesized palladium nanoparticles as effective catalysts for the Suzukicoupling reactionsin aqueous media, *Journal of Saudi Chemical Society,* Vol.21 (4): 450-457, 2017.

116.   S. R. Senthilkumar , and T. Sivakumar. Green tea (Camellia sinensis) mediated synthesis of zinc oxide (ZNO) nanoparticles and studies on their antimicrobial activities, *Int J Pharm Pharm Sci,* **Vol. 6.6**: 461-465, 2014.

117.   A. M. Awwad, N. M. Salem and A. O. Abdeen. Green synthesis of silver nanoparticles using carob leaf extract and its antibacterial activity, *International Journal of Industrial Chemistry* , Vol. **4**: 29, 2013.

118.   K. M. Kumar, B. K. Mandal, K. S. Kumar, P. S. Reddy, and B. Sreedhar. Biobased green method to synthesise palladium and iron nanoparticles using Terminalia chebula aqueous extract , *Spectrochim. Acta: Spectrochimica Acta Part A: Molecular and Biomolecular Spectroscopy*, Vol.102: 128-133, 2013.

119.   M. A. Chougule, S. G. Pawar, P. R. Godse, R. N. Mulik, S. Sen and V. B. Patil. Synthesis and Characterization of Polypyrrole(PPy) Thin Films, *Soft Nanoscience Letters* **Vol.1 No.1**: 5, 2011.

120.   M. Sharma, G. I. Waterhouse, S. W. Loader, S. Garg and D. Svirskis. High surface area polypyrrole scaffolds for tunable drug delivery*, International Journal of Pharmaceutics* , Vol.**443**: 163- 168, 2013.

Bibliography

121.   S. M. Reda, and M. G. Sheikha. Synthesis and Electrical Properties of Polyaniline Composite with Silver Nanoparticles. *Advances in Materials Physics and Chemistry, Vol.***2**: 75-81, 2012.